A Measurement of

$$\frac{BR\left(D_S^\pm \to f_0(980)\pi^\pm\right)}{BR\left(D_S^\pm \to \phi(1020)\pi^\pm\right)} \cdot \frac{BR\left(f_0(980) \to K^+K^-\right)}{BR\left(\phi(1020) \to K^+K^-\right)}$$

in Fermilab E791

by

JAMES NORRIS

BS in Physics, Metropolitan State College of Denver, 1993

BA in Philosophy, Metropolitan State College of Denver, 1993

A THESIS

Submitted in partial fulfillment of the

requirements for the degree

MASTER OF SCIENCE

Department of Physics

College of Arts and Sciences

KANSAS STATE UNIVERSITY

Manhattan, Kansas

1996

Approved by: _____
                        Major Professor

ABSTRACT

The product of the ratios of the branching fractions:

$$BR(D_S^\pm \to f_0(980)\pi^\pm) \cdot BR\big(f_0(980) \to K^+K^-\big) / BR(D_S^\pm \to \phi\pi^\pm) \cdot BR\big(\phi \to K^+K^-\big)$$

in Fermilab E791 is measured. A gaussian curve is fit to the invariant mass plots of $K^+K^-\pi^\pm$ to identify the $D_S^\pm$. Invariant mass plots of K^+K^- are fit with a Breit-Wigner curve to identify the ϕ and the WA76 parameterization of the $f_0(980)$ is used to identify the $f_0(980)$. In order to determine the detector efficiency for the decay $D_S^\pm \to f_0(980)\pi^\pm$, the Monte Carlo mass generation routine, ULMASS.F of Jetset 7.4, is modified to include the WA76 parameterization to generate the appropriate line-shape for the decay $f_0(980) \to K^+K^-$.

Table of Contents

Chapters   Page

List of Figures

List of Tables

Dedication

For my father:

Perhaps more than he expected, but probably less than he hoped.

To KSU HEP:

No more than was necessary, and far less than was possible.

Acknowledgments

There are many people and one animal that I'd like to thank for their help and support through last three years. First and foremost, my wife, Junell. And Jessie, my puppy - not Jesse Goldman, though he also deserves thanks for many hours of amusement at Arun Tripathi's expense, who in turn deserves thanks for the Feynman diagrams that grace this thesis - who made me feel as though I was the most wonderful person in the world, even when I didn't feel that way myself.

Then there's Professor Larry Weaver, who treats any and all questions, no matter how basic, as though they are interesting and worthy of deep contemplation. A nicer person and better teacher I could not hope to know.

I'd also like to thank Dr Torbjorn Sjostrand, author of Pythia and Jetset, who doesn't know me from Adam, but who, even so, expended no small effort in helping me figure out how to modify Jetset so as to produce the correct lineshape for the $f_0(980)$ - this analysis would seem a waste of time to me if not for this. Also Rodney Greene, who I've never spoken with, *via* any medium, but without whose thesis I would not have known what lineshape to give the $f_0(980)$ in the first place.

And finally Daniel Mihalcea, who told me as I was working on the final draft of this thesis to think of this thesis, not as *the* end, but the end of a chapter, or perhaps a prologue.

Vita

James Norris received a BS in Physics and a BA in Philosophy from Metropolitan State College of Denver, (Denver, Colorado) in the spring of 1993. While working on his undergraduate degrees, he participated in the first Summer Resarch Experience for Undergraduates in the James R McDonald Atomic Physics Laboratory at Kansas State University (Manhattan, Kansas), where he worked with Professor Itzik Ben-Itzahk on the fragmentation of methane due to the impact of fast protons in the summer of 1992. He also worked at Brookhaven National Laboratory (Upton, New York) in the spring and summer of 1993 with Flemming Videbaek on developing software to analyze the output of a pixellatd Ring Imaging Cherenkov Detector for the BRAHMS experiment at the Relativistic Heavy Ion Collider (RHIC). While at KSU, he worked at KSU and Fermi National Lab on the testing, installation, and balancing of the over 600 photomultipliers for the E815 detector. In hopes of becoming a better physicist, he is now pursuing MS in Mathematics at KSU. As time allows, he continuous to take the occasional course in philosophy. His publications and presentations include:

JOURNAL PUBLICATIONS

1. *In-beam tests of a ring imaging Cherenkov detector with a multianode photomultiplier readout*, with R Debbe *et al*, Nuclear Instruments and Methods in Physics Research A 362 (1995) 253-260.

2. *Velocity Dependence of ionization and fragmentation of methane caused by fast-proton impact*, with I Ben-Itzhak *et al*, Physical Review A 49(1994) 881-888.

3. *Direct Determination of Recoil Detection Efficiency for Coincidence Time-of Flight Studies of Molecular Fragmentation*, with I Ben-Itzhak *et al*, Nuclear Instruments and Methods in Physics Research B 79 (1993) 138-141.

4. *Fragmentation of CH_4 by Fast Protons*, with I Ben-Itzhak *et al*, Physics Review A 47 (1993) 3748-3757.

CONFERENCE PROCEEDINGS

1. *Velocity Dependence of the Fragmentation of Methane by Fast Proton Impact*, with I Ben-Itzhak *et al.*, Proceedings of the VIth International on the Physics of Highly Charged Ion Conference, Kansas State University, Manhattan, Kansas, edited by P Richard, M Stockli, C Cocke, and C Lin, 339 (1993) 339-342.

CONFERENCE PRESENTATIONS (PAPER)

1. *Computers, Minds, Understanding Language, and this Kinda Fuzzy Concept Called Intentionality*, J Norris, at the 1st Annual Graduate Interdisciplinary Forum, Kansas Satet University, Manhattan KS, April 20 1996.

2. *Computers, Minds, Understanding Language, and this Kinda Fuzzy Concept Called Intentionality*, J Norris, at the 19th Annual Meeting of the New Mexico & West Texas Philosophical Society, University of Texas at Austin, Austin TX, April 8 1996.

3. *The Problem with Philosopher-Kings*, J Norris, at the 18th Annual Meeting of the New Mexico & West Texas Philosophical Society, University of Texas at El Paso, El Paso TX, April 16 1995.

4. *Causal Laws, Natural Laws, and Lewis' Theory of Counterfactuals*, J Norris, at the 17th Annual Meeting of the New Mexico & West Texas Philosophical Society, University of Texas at El Paso, El Paso TX, April 161994.

CONFERENCE PRESENTATIONS (POSTER)

1. *Direct Determination of Recoil Detection Efficiency for Coincidence Time-of-Flight Studies of Molecular Fragmentation*, J Norris, at the XI Applications of Accelerators in Research and Industry, Denton, TX, November 6, 1992.

COLLOQUIA AND SEMINARS

Kansas State University, Manhattan KS
Brookhaven National Laboratory, Upton NY
Metropolitan State College of Denver, Denver CO
University of Colorado at Denver, Denver CO

Chapter 1 - Introduction

Particles, say, for example, the $f_0(980)$, are said to have a particular rest-mass, in this case 980 MeV. But such particles are allowed to decay into two other particles, *e.g.* a K^+ and a K^-, whose rest-mass sum is 988 MeV. This kind of 'below-threshold' decay is possible in high energy physics because the mass of a particle is approximately distributed along a Breit-Wigner curve (BW), see *Figure 4.1*, and the mass that is often quoted as the particle's mass is really the central or most likely mass of this distribution. For some $f_0(980)$, the width of this curve allows them to have a mass greater than the 988 MeV rest-mass of the K^+K^- pair. Thus, the decay $f_0(980) \to K^+K^-$ is kinematically allowed.

The width of the BW curve has another physical significance: for each decay mode, the width of the curve is directly related to the rate at which the particle will decay by the Uncertainty Principle: $\Delta E \Delta t = \hbar$. If $\Delta E = (\Delta m)c^2$ where Δm is the width of the BW curve and $\Delta t = \tau$ is the lifetime, then $\tau = \hbar / (\Delta m)^2 c$. For the vast majority of particle decays, *i.e.* those where the decaying particle is significantly more massive than the decay products, the lineshape of one decay mode is the same as all others. But when, as is the case for $f_0(980) \to K^+K^-$, this is not true, the BW curve becomes distorted, see *Figure 4.2*, and the decay rate of below- or near-threshold decays can vary from those of other decay modes. In any case, when the BW curves for all the particle's decay modes are added together, the resulting width is directly related to particle's life-time by the Uncertainty Principle, as above.

Experimentally, the distinctively symmetric BW peak in an invariant mass plot of the decay daughter particles identifies the presence of a parent particle's decay. The invariant mass of two (or more) particles is plotted in a histogram, and if they are the decay products from some parent particle, a BW peak will be

apparent: a maximum value will occur at (or near) the central mass of the decaying particle, and to limit of the detector's mass-resolution, the width of the this peak will be the width of the decaying particle.

Troubles occur, however, when the decay is below threshold, as is the case for $f_0(980) \to K^+K^-$. In cases like these, what is seen in the plot is not a BW, with a well-defined maximum and width, but instead a product of the underlying BW and the phase-space available for the decay. The curve is no longer symmetric, and thus both the width and central value are not well-defined.

Due to its lack of phase space in this mode, the exact composition of the $f_0(980)$ is still uncertain. Various studies have characterized it as: a conventional $q\bar{q}$ meson [Morgan(1974), Törnqvist], a multiquark state [Jaffe(1977)], a $K\overline{K}$ molecule [Weinstein], a glueball [Jaffe(1975), Robson], and a hybrid [Barnes]. While the most recent studies conclude that the $f_0(980)$ is simply a conventional $q\bar{q}$ meson [Morgan(1993)], the various possibilities and challenges involved in studying a below-threshold decay such as $f_0(980) \to K^+K^-$ make the $f_0(980)$ quite fascinating.

To study the $f_0(980) \to K^+K^-$, one needs large numbers of the $f_0(980)$, and one way to produce such numbers is to create large numbers of particles which decay to the $f_0(980)$. Such a particle is the $D_S^\pm$, a charm meson (D_S^+: $c\bar{s}$, D_S^-: $\bar{c}s$), which decays: $D_S^\pm \to f_0(980)\pi^\pm$. Fermilab Experiment 791 (E791) produced more charm than any previous hadroproduction experiment. As a result, many light-flavor meson decay modes are available for study in copious quantities. Because the $f_0(980)$ is below the K^+K^- threshold, large numbers of the $f_0(980)$ are necessary to be able to perform any sort of serious study of this particle. E791's high statistics make such a study worth attempting.

Chapter 2 - Motivation

Gell-Man's development of the Eight-Fold Way in 1961 [Gell-Mann] and the subsequent quark model allowed, for the first time, a systematic understanding of the plethora of particles produced in high energy interactions. Baryons and mesons were proposed to be made of elemental, spin 1/2 fermions called quarks. We now think there are six such quarks, grouped into three families, which are classified on the basis of charge and mass; see *Table 2.1*.

charge	Family 1		Family 2		Family 3	
	flavor	mass (MeV)[1]	flavor	mass (MeV)	flavor	mass (GeV)
+2/3	up	310	charm	1600	top	170
-1/3	down	310	strange	483	bottom	5

Table 2.1 - The Quarks

Each of these quarks has an anti-quark partner. Baryons are composed of three quarks or three antiquarks, and mesons are made up of a quark and an anti-quark. The mesons in turn are grouped into nonets (*i.e.* nine mesons each), an SU(3)-flavor octet and its singlet partner. As such, the nonets are defined by each meson having the same angular momentum, parity, and charge conjugation quantum numbers, written as J^{PC}. These numbers are defined, respectively:

$$J=|\mathbf{L}+\mathbf{S}| \qquad\qquad P=(-1)^{L+1} \qquad\qquad C=(-1)^{L+S}$$

where L≡orbital angular momentum of the two quarks relative to one another, and S≡intrinsic spin of the two quarks taken together.

---

[1] These masses are somewhat hypothetical - the Standard Model of the Quark Theory does not allow quarks to exist independently, *i.e.* they are constrained to appear only as mesons or baryons (see below). But for the proton, whose quark content is uud and whose mass is ~938 MeV, and other light hadrons these mass assignments make naive sense.

One would expect that the nonet with the 'smallest' J^{PC} quantum numbers would be composed of the lightest mesons, and that as the J^{PC} numbers of the nonets increase, so would the masses of their mesons.

The six lowest-lying nonets, which are generated from **L**=0,1 and **S**=0,1, are presented in *Table 2.2*. One will notice that, as mentioned above, the 3 nonets

orbital angular momentum	L=0		L=1			
spin	s=0	s=1	s=0	s=1	s=1	s=1
J^{PC}	0^{-+}	1^{--}	1^{+-}	0^{++}	1^{++}	2^{++}
typical masses (MeV)	500	800	1250	1150	1300	1400
$^{2S+1}L_J$	$^{1}S_0$	$^{3}S_1$	$^{1}P_1$	$^{3}P_0$	$^{3}P_1$	$^{3}P_2$

Table 2.2 - Quantum Numbers of the 6 Lowest-Lying Nonets

with lowest masses are the L=0 0^{-+} psuedoscalars and 1^{--} vectors, and finally the L=1 0^{++} scalars. Two of these three nonets are well understood: the psuedoscalars and vectors, see *Figure 2.1*.

$$\pi^0 = \frac{1}{\sqrt{2}}\left(u\bar{u} - d\bar{d}\right)$$

$$\eta = \frac{1}{\sqrt{6}}\left(u\bar{u} + d\bar{d} - 2s\bar{s}\right) \quad \eta' = \frac{1}{\sqrt{3}}\left(u\bar{u} + d\bar{d} + s\bar{s}\right)$$
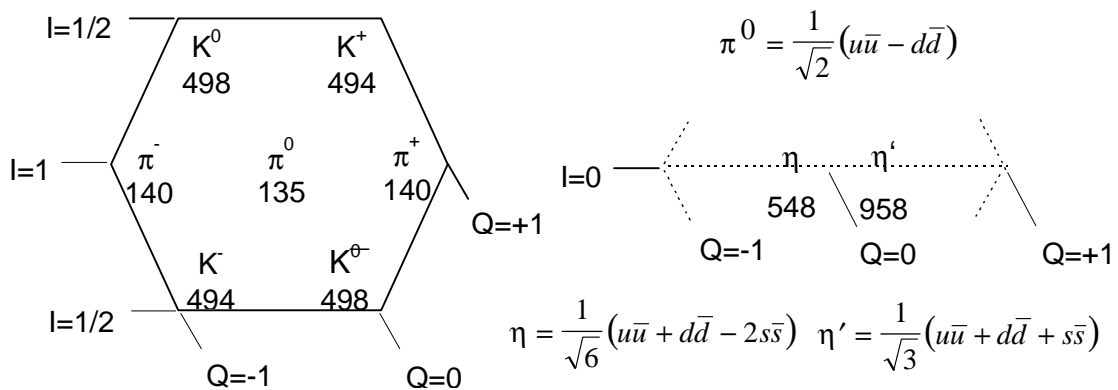
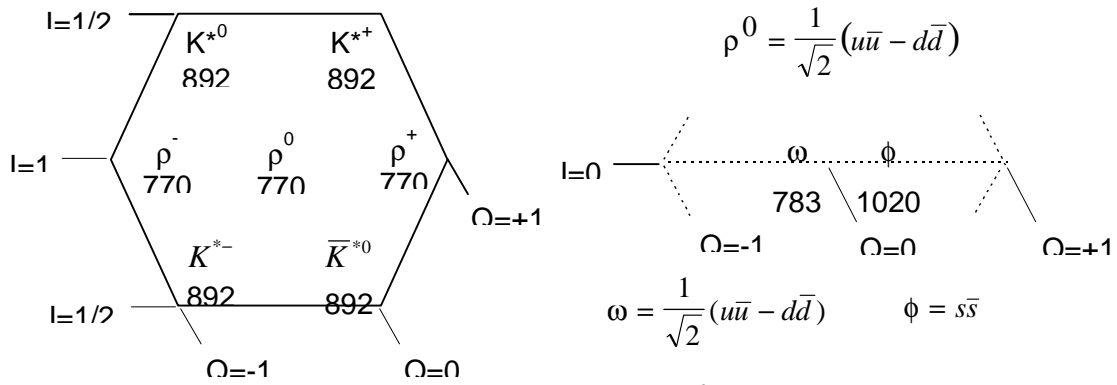Figure 2.1a - The PseudoScalar (0^{-+} or $^{1}S_0$) Nonet

Figure 2.1b -The Vector (1^- or $^3S_1$) Nonet

Note: Isospin (I) is indicated on the horizontal, charge (Q) on the diagonal, masses in MeV under the particle name, and the quark content of the neutral I=0 and I=1 particles are listed. The neutral I=0 particles are displaced to the right for clarity.

There are several things to notice in *Figure 2.1*. Most important to the present discussion is the mixing of quarks for the neutral mesons of these two nonets. For the pseudoscalars, the I=0 η and η' are mixtures of all three light quarks, with the η being 'more' strange than the η', but still being a superposition of all three of the light quarks. On the other hand, the vector (I=0) ω and ϕ are said to be 'ideally mixed', *i.e.* the ω has no strange quark content while the ϕ is nothing but strange. This assignment is arrived at from a number of observations which will later apply to the $f_0(980)$. First: the ϕ decays into kaons and pions - the branching fraction for $\phi \to \rho^\pm \pi^\mp$ is only 0.13 while $\phi \to K\overline{K}$ is 0.84 giving a ratio of branching ratios $BR(\phi \to \rho^\pm \pi^\mp)/BR(\phi \to K\overline{K}) = 0.15$. The most likely explanation for this disparity in branching fractions is the quark
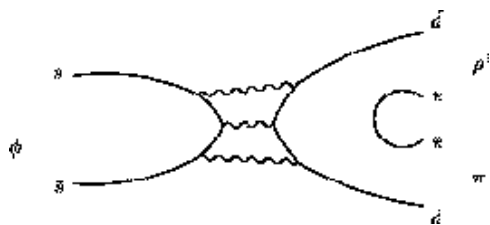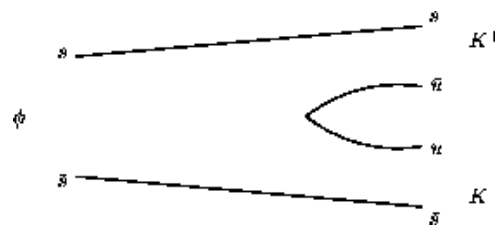

Figure 2.2a - $\phi \to \rho^\pm \pi^\mp$

Figure 2.2b - $\phi \to K^+ K^-$

5

content given above in *Figure 2.1b*. That is, with only $s\bar{s}$, the $\phi \rightarrow \rho^{\pm}\pi^{\mp}$ decay is Okuba-Zweig-Iizuka (OZI) suppressed [Griffiths, pg 75]; see *Figure 2.2*. The mass of the ϕ is 1020 MeV, and the masses of the daughters is in these two cases, $\phi \rightarrow \rho^{\pm}\pi^{\mp}$ and $\phi \rightarrow K\overline{K}$, are 910 MeV (770 MeV + 140 MeV) and 992 MeV (494 MeV + 498 MeV), respectively. As a result, $\phi \rightarrow \rho^{\pm}\pi^{\mp}$ has ~110 MeV phase space and $\phi \rightarrow K\overline{K}$ has ~30 MeV. These decays are relativistic, so $E^2 = p^2 + m^2$ and the phase space is proportional to $\dfrac{d^3p}{2EdE} = \dfrac{p^2}{2E}\dfrac{dp}{dE}d\Omega$. Solving the former for $\dfrac{dp}{dE} = \dfrac{E}{p}$ and substituting this into the latter yields:

$$\frac{d^3p}{2EdE} = \frac{p^2}{2E}\left(\frac{E}{p}\right)d\Omega = \frac{p}{2}d\Omega.$$ As the ratio of rates or branching fractions for $\phi \rightarrow \rho^{\pm}\pi^{\mp}$ and $\phi \rightarrow K\overline{K}$ will go as the ratio of phase space times the ratio of the matrix elements squared for the two, the ratio of branching fractions will go as the ratio of the momenta times the ratio of the square of the matrix elements of the two decays. $p = {\sim}180$ MeV and $p = {\sim}120$ MeV for $\phi \rightarrow \rho^{\pm}\pi^{\mp}$ and $\phi \rightarrow K\overline{K}$, respectively. Thus, the ratio of branching fractions $BR\left(\phi \rightarrow \rho^{\pm}\pi^{\mp}\right)\big/BR\left(\phi \rightarrow K\overline{K}\right)$ one would expect would be $\dfrac{180\,MeV}{120\,MeV} = \dfrac{3}{2} = 1.5$. The matrix element for $\phi \rightarrow \rho^{\pm}\pi^{\mp}$ will differ from that of $\phi \rightarrow K\overline{K}$ by at least a factor due to OZI suppression. If OZI is good for a factor of 5 or 6 or 7 suppression, then $BR\left(\phi \rightarrow \rho^{\pm}\pi^{\mp}\right)\big/BR\left(\phi \rightarrow K\overline{K}\right)$ goes from 1.5 to something on the same order of magnitude of $0.15\phi \rightarrow \rho^{\pm}\pi^{\mp}$. So one concludes that the ϕ is more $s\bar{s}$ than not.

The argument for the ideal mixing of the ω and ϕ proceeds by noting the difference in their masses, also as indicated in *Figure 2.1b*. Recalling the QED hyperfine splitting formula (*i.e.* spin-spin coupling in the hydrogen atom) [Griffith, pg 172]:

$$\Delta E_{hf} = \frac{8\pi\gamma_p e^2}{3m_e m_p c^2}\left(\bar{S}_1 \cdot \bar{S}_2\right)\left|\psi_{100}(0)\right|^2,$$ (2.1)

one might guess that there would be similar spin-spin coupling in QCD:

$$mass(q_1\bar{q}_2) \approx m_1 + m_2 + \left(\frac{2m_u}{\hbar}\right)^2\left(160 MeV/c^2\right)\left(\frac{(\vec{S}_1 \cdot \vec{S}_2)}{m_1 m_2}\right).$$ (2.2)

Using the arguably naive *(2.2)* , one can make surprisingly accurate predictions for the masses of pseudoscalar and vector mesons; see *Table 2.3*:

Nonet	pseudoscalar: $\vec{S}_1 \cdot \vec{S}_2 = -\frac{3}{4}\hbar^2$			vector: $\vec{S}_1 \cdot \vec{S}_2 = \frac{1}{4}\hbar^2$			
particle	K	π	η	K^*	ρ	ω	ϕ
calculated mass (MeV)	484	140	559	896	780	780	1032
observed mass (MeV)	496	138	549	892	776	783	1020

Table 2.3 - Calculated and Observed Masses for Pseudoscalar and Vector Mesons

These theoretical predictions are quite good[2], and indicate that the ϕ is pure $s\bar{s}$. Thus, the pseudoscalar and vector nonets are quite different, at least in respect to their two I=0 neutral mesons - the pseudoscalars are each a mixture of all three light quarks, while the vectors are ideally mixed. So the question is, what should be expected of the scalar mesons?

For various reasons, the spectroscopy of the scalars is not as clear. First, as the mass of the mesons increases, so do their widths - and this leads to one scalar meson overlapping another. Secondly, scalars seem as a rule to couple strongly to multiple channels, often to channels that are close to, or even below-threshold, as is the case for $f_0(980) \to K^+ K^-$. For a more thorough discussion of the scalar mesons as a group, see the PDG [PDG(1996), pg 1478].

---

[2] One will note that the η' is not presented in *Table 2.3* - for an explanation as to why not, see C Quigg, <u>Gauge Theories of the Strong, Weak, and Electromagnetic Interactions</u>, (Benjamin, New York, 1983), pg 252.

What is known about the $f_0(980)$ is that it couples strongly to both $K\overline{K}$ and $\pi\pi$, and that it is isospin 0. This means there should be another isospin=0 partner, as the η and η' are isospin=0 pseudoscalar partners and the ω and ϕ are isospin=0 vector partners. The $f_0(1370)$ has been tentatively identified as its partner, but there are problems with this assignment, see *Table 2.4*.

particle	mass (MeV)	width (MeV)	$\Gamma_{\pi\pi}/\Gamma_{total}$	$\Gamma_{4\pi}/\Gamma_{total}$	$\Gamma_{K\overline{K}}/\Gamma_{total}$
$f_0(980)$	980±10	40-100	0.781±0.024	not seen	0.219±0.024
$f_0(1370)$	1200-1500	300-500	<0.15-0.20	0.80±.04	seen

Table 2.4 - The $f_0(980)$ and $f_0(1370)$

The mass of these scalar mesons cannot be as easily predicted as the pseudoscalars and vectors, because in this case neither the orbital angular momentum nor spin are zero. But the branching fractions are suggestive: the $f_0(1370)$ is at least four times more likely to decay to pions than kaons, and the $f_0(980)$, which is below the KK threshold, decays to $K\overline{K}$ a significant portion of the time. This would seem to indicate that the $f_0(1370)$ is mostly up and down quarks, as was the ω, and the $f_0(980)$ is mostly strange, like the ϕ.

The masses of the two seem to contradict this conclusion: one would expect the 'mostly strange' $f_0(980)$ to be heavier than the $f_0(1370)$. There are several possible answers to this quandary, *e.g.* one or both of the $f_0(980)$ and $f_0(1370)$ have been misidentified as standard mesons. The *correct* answer, of course, will not be discovered unless more experimental data on the $f_0(980)$ is collected.

Chapter 3 - Previous Work

Because the decay $f_0(980) \to K^+ K^-$ is below-threshold, this decay is not very well characterized at present. In the 1994 PDG [PDG(1994), p1464] the central mass was listed as 980±10 MeV and the width was 40-400MeV! In the 1996 PDG [PDG(1996), p338] the width has been improved to 40-100 MeV. The uncertainty in the width is still quite significant, and due predominately to the low statistics currently available in the $f_0(980) \to K^+ K^-$.

As mentioned above, many studies have been made, and many models of the $f_0(980)$ advanced. The most complete is a 'resonance pole topology' study by Morgan, *et al* [Morgan(1993)], in which the authors conclude that the $f_0(980)$ is a standard, narrow ($\Gamma_0 \approx 52$ MeV) Breit-Wigner resonance, but which is most likely not a $q\bar{q}$ meson. Perhaps it is the lightest glueball [Jaffe(1977)] or a scalar excitation of Gribov's QCD vacuum [Gribov].

Setting aside questions of the composition and nature of the $f_0(980)$, R. Greene's PhD thesis [Greene] currently presents the most thorough analysis available of the $D_S^{\pm} \to K^+ K^- \pi^{\pm}$ decay mode, employing a Dalitz plot analysis to extract decay fractions and relative phases for both three- and two-body resonant decays. Of interest to the current work is the WA76 parameterization of the $f_0(980)$ [WA76] presented in Greene's thesis [Greene, p145] - this parameterization will be presented in the next chapter.

Chapter 4 - Theory

4.1 Parameterization of the f_0(980)

As mentioned above, R Greene's PhD thesis is to date the most comprehensive study of the $D_S^\pm \to K^+ K^- \pi^\pm$ decay mode, and in it he analyzed several different parameterizations of the $f_0(980)$ [Greene, p145], but settled on the WA76 parameterization [WA76] as the most suitable for $D_S^\pm \to \left(f_0(980) \to K^+ K^- \right) \pi^\pm$. For this reason, the WA76 parameterization of the $f_0(980)$ is used here.

Table 4.1 gives the functional form and constants of the WA76 parameterization:

Forms	Constants
$\mathcal{M}_{f_0(980)} = \dfrac{1}{m_0^2 - m^2 - i m_o (\Gamma_k + \Gamma_\pi)}$	m_0=979 MeV
$\Gamma_\pi = g_\pi \sqrt{\dfrac{m^2}{4} - m_\pi^2}$	g_π=0.28±0.04
$\Gamma_K = \dfrac{g_K}{2} \left(\sqrt{\dfrac{m^2}{4} - m_{K^+}^2} + \sqrt{\dfrac{m^2}{4} - m_{K^0}^2} \right)$	g_K=0.56±0.18

Table 4.1 - WA76 $f_0(980)$ Parameterization

The matrix element of *Table 4.1* yields, when squared, the standard, symmetric (but un-normalized) Breit-Wigner formula:

$$BW = \frac{1}{\left(m_0^2 - m^2\right)^2 + m_0^2 \left(\Gamma_K + \Gamma_\pi\right)^2}$$

However, the fact that the $f_0(980)$ is below-threshold for the K⁺K⁻ decay introduces an asymmetry into the BW curve describing $f_0(980)$ decay; see
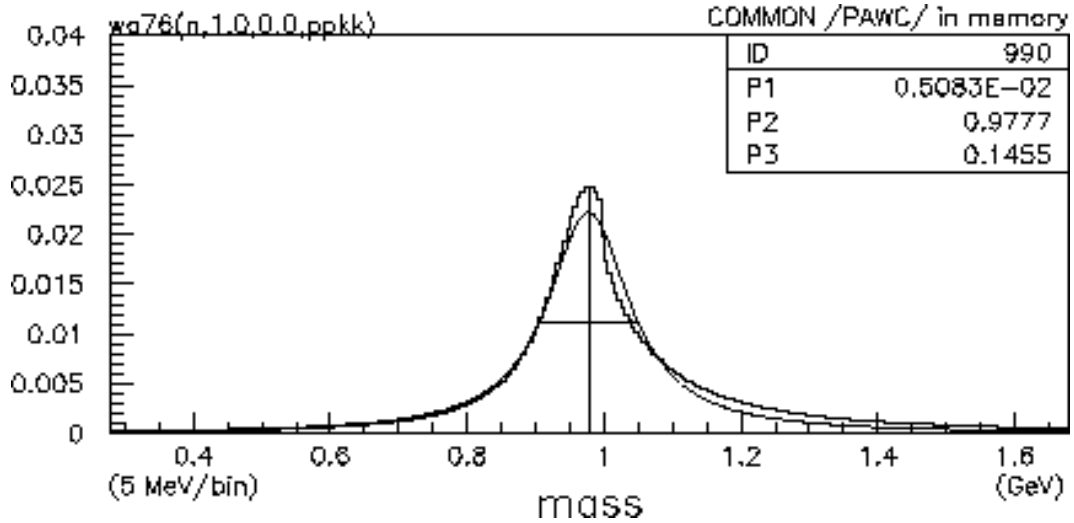
Figure 4.1 - The WA76 f₀(980) Parameterization and Gaussian Fit

Note: The vertical and horizontal lines mark the central mass value (*P1*) and HWHM
(*P3*), respectively.

Figure 4.1.   *Figure 4.1* is the total $f_0(980)$ line shape, *i.e.* the sum of the line

shapes for $f_0(980) \rightarrow K^+K^-$ and $f_0(980) \rightarrow \pi^+\pi^-$

If fit with a standard BW, the WA76 $f_0(980)$ appears to have a central-mass

value of 979 MeV (*P1*), and a width of 145.5 MeV (*P3*).   If one plots *only* the

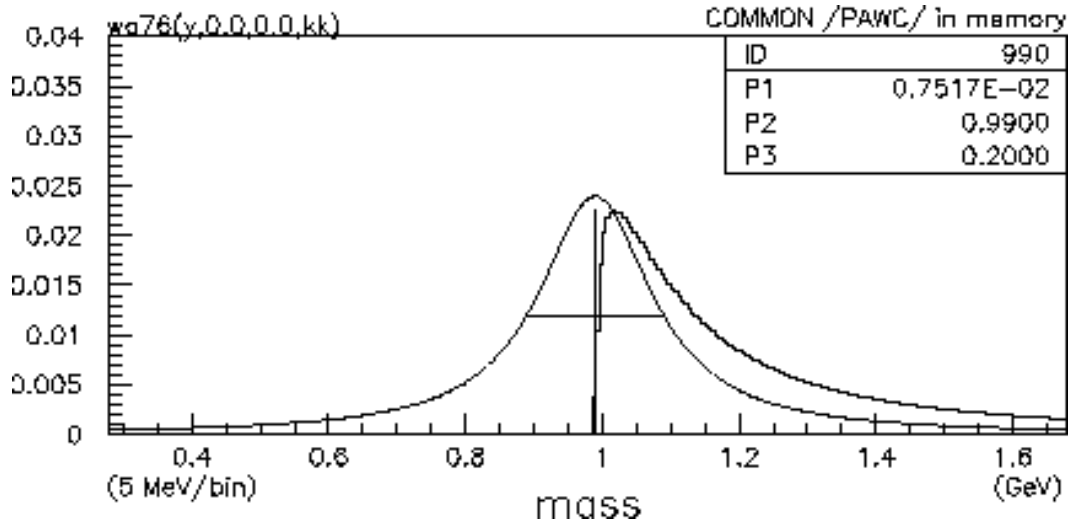number of $f_0(980) \rightarrow K^+K^-$ as a function of the invariant mass of the K^+K^- pair,

Figure 4.2 - The $f_0(980) \rightarrow K^+K^-$ Line Shape and Gaussian Fit

then *Figure 4.2* results. The best possible BW fit is also shown, in *Figure 4.2*, and is clearly absurd.

4.2 The Decay $D_S^{\pm} \rightarrow K^+K^-\pi^{\pm}$

The $D_S^{\pm}$ is described in the '96 PDG [PDG(1996), p471], see *Table 4.2*.

quark content:	mass (MeV):	lifetime (psec):	quantum numbers:
$D_s^+ = c\bar{s}$ $D_s^- = \bar{c}s$	1968.5±.06	.467±.017	$I(J^P)=0(0^-)$
Total (%)	Resonant (%)		Non-resonant (x10^{-3})
$\dfrac{\Gamma(K^+K^-\pi^{\pm})}{\Gamma} = 4.6 \pm 1.2$	$\dfrac{\Gamma(\phi\pi^{\pm})}{\Gamma} = 3.6 \pm 0.9$	$\dfrac{\Gamma(f_0(980)\pi^{\pm})}{\Gamma} = 1.1 \pm .04$	$\dfrac{\Gamma(K^+K^-\pi^{\pm})}{\Gamma} = (9 \pm 3)$

Table 4.2 - The $D_S^{\pm}$

The $D_S^{\pm}$ can decay to $K^+K^-\pi^{\pm}$ *via* a Cabibbo-favored (*i.e.* quarks of one family decaying to quarks of the same family) weak decay. When it does so, it is possible for the decay to proceed immediately to $K^+K^-\pi^{\pm}$, or to proceed *via* an intermediate decay: $D_S^{\pm} \rightarrow X^0\pi^{\pm}$, where the X^0 is some neutral particle which can itself decay to K^+K^-. Feynman diagrams for these two processes are
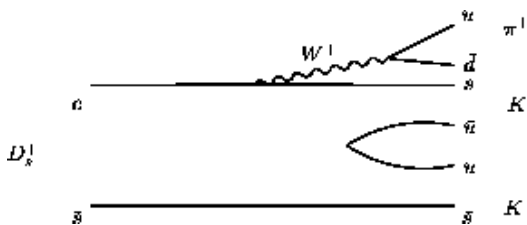

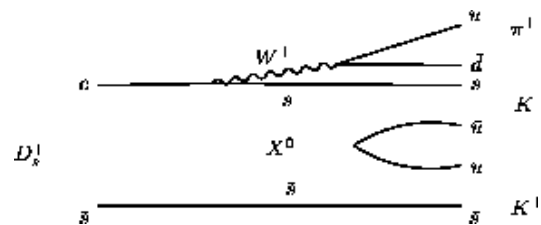Figure 4.3a - Feynman Diagram of $D_S^{\pm} \rightarrow K^+K^-\pi^{\pm}$

Figure 4.3b - Feynman Diagram of $D_S^{\pm} \rightarrow \left(X^0 \rightarrow K^+K^-\right)\pi^{\pm}$

shown in *Figure 4.3*.

Assuming that there is more than one actual particle that can stand in the place of the hypothetical X^0, and that these particles can be distinguished by

some means, *e.g.* their peaks are separated sufficiently to be identified by a plot of the invariant mass of the K^+K^-, one might wonder what the ratio of the branching ratios for the two particles is. As it happens, both the ϕ and $f_0(980)$ meet these criteria. The ratio of the number of $D_S^\pm \to \phi\pi^\pm$ and $D_S^\pm \to f_0(980)\pi^\pm$ is given by *Equation (4.1):*

$$\frac{\#of\left(D_S^\pm \to f_0(980)\pi\right)}{\#of\left(D_S^\pm \to \phi\pi\right)} = \frac{\sigma\left(D_S^\pm\right)\cdot BR\left(D_S^\pm \to f_0(980)\pi\right)\cdot BR\left(f_0(980) \to K^+K^-\right)\varepsilon_{f_0}}{\sigma\left(D_S^\pm\right)\cdot BR\left(D_S^\pm \to \phi\pi\right)\cdot BR\left(\phi \to K^+K^-\right)\varepsilon_\phi}, \quad (4.1)$$

where $\sigma\left(D_S^\pm\right)$ is the cross-section of producing $D_S^\pm$, and ε_ϕ and ε_f are the efficiencies of detected the ϕ and $f_0(980)$, respectively. Notice that the $D_S^\pm$ cross-section is common to both numerator and denominator, and cancels out. The product of the ratio of branching ratios is then:

$$\frac{BR\left(D_S^\pm \to f_0(980)\pi^\pm\right)}{BR\left(D_S^\pm \to \phi\pi^\pm\right)} \cdot \frac{BR\left(f_0(980) \to K^+K^-\right)}{BR\left(\phi \to K^+K^-\right)} = \frac{\#of\left(D_S^\pm \to \phi\pi^\pm\right)}{\#of\left(D_S^\pm \to f_0(980)\pi^\pm\right)} \cdot \frac{\varepsilon_\phi}{\varepsilon_{f_0(980)}} \quad (4.2)$$

Chapter 5 - Experiment E791

5.1 The E791 Experimental Setup

Experiment E791 was located at Fermi National Accelerator Laboratory (FNAL) in Batavia IL, and ran as a fixed-target experiment from June 1991 to January 1992. A 500 GeV π^- beam was created by the Fermilab accelerator in the following process; see *Figure 5.1* for a schematic drawing of the Fermilab Accelerator and beamlines. (A detailed description of the Fermilab accelerators can be found elsewhere; see [Witchey, pg 15].)

First, 'spills' of approximately 2×10^{12} protons were accelerated to 750 KeV in a Cockcroft-Walton electrostatic accelerator and injected into the LINAC where they were boosted to 200 MeV. Second, a rapid-cycling synchrotron boosted them to 8 GeV followed by a boost to 150 GeV in the old main ring. Third, the protons were boosted to the full 800 TeV in the superconducting main ring. They were then extracted and sent to the fixed-target switchyard, where they were directed to the individual experiments. Spills of approximately 10^7 500 GeV π^- were then created when these protons interacted with a 30 cm-long
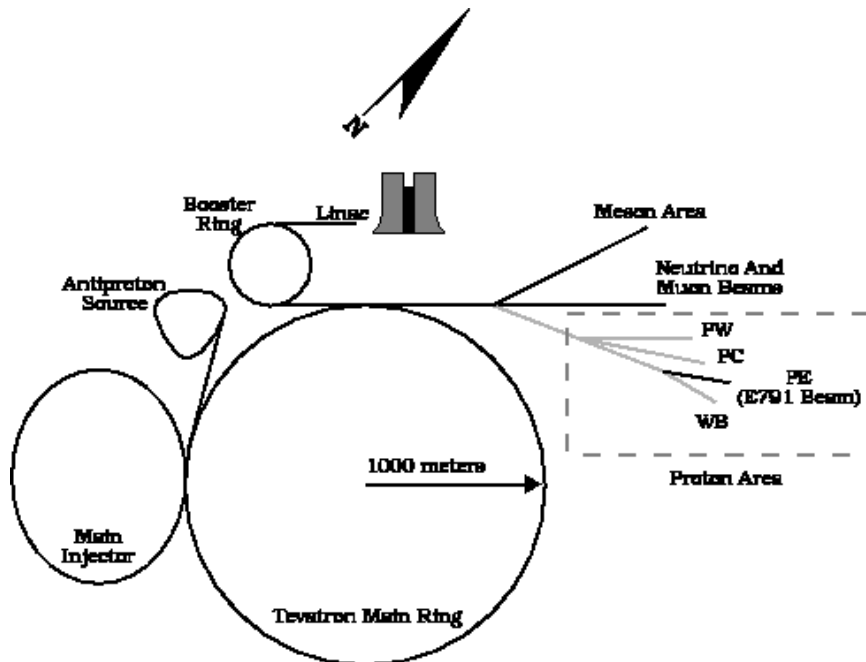

Figure 5.1 - Fermilab Accelerators and Beamlines

Beryllium primary target. These π^- were then directed to the E791 secondary target. Each spill of π^- was 22 seconds in duration and was followed by an 'interspill' of 35 seconds during which the accelerator ramped back up for the next spill.
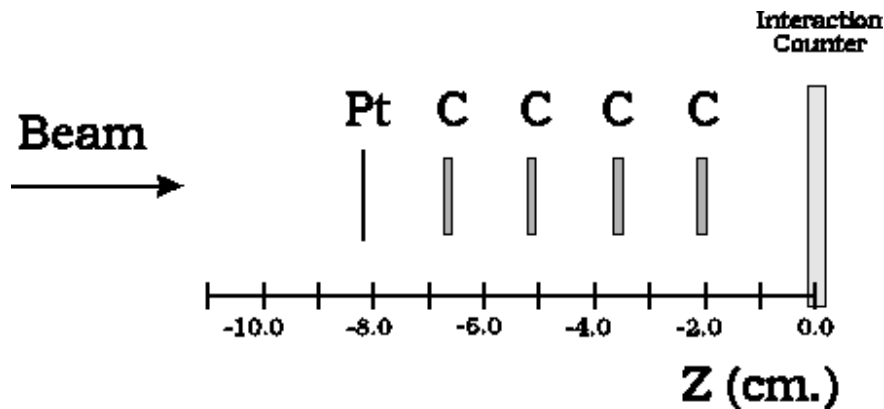

Figure 5.2 - E791 Secondary Target Foils

For E791, the secondary target was a platinum $50 Australian coin followed by four carbon foils milled from industrial diamond drill bits, see *Figure 5.2*. Spacing between the foils was determined by the decay length, $\ell=\gamma\beta c\tau$, of a typical charm particle, say the $D^\pm$ with a $\tau=5\times10^{-13}$ sec and where the meson is produced with a momentum of 70 GeV (thus $\gamma=37$ and $\beta\approx1$ for $c=3\times10^{10}$ cm/sec). Thus $\ell=1.1$ cm, and the foils were spaced 1.5 cm apart so as to allow the charm mesons produced to decay before encountering the next foil.

A detailed description of the E791 detector can be found elsewhere [Witchey, pg 19], so the following description be brief; see *Figure 5.3* for a schematic drawing of the detector. The E791 detector comprised a spectrometer originally built for the photoproduction charm experiment E516 which ran in the early 1980s. This spectrometer was then upgraded three times for subsequent charm experiments: E691 (photoproduced charm), E769 and E791 (both of which were hadroproduced charm).
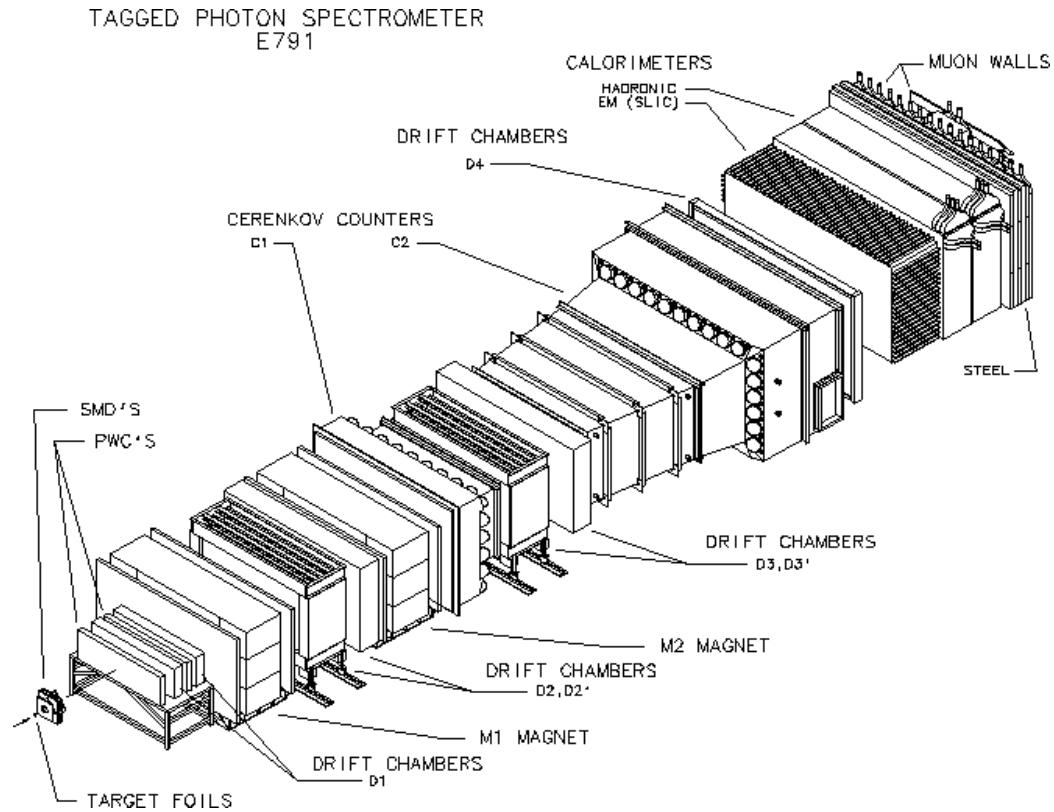
Figure 5.3 - E791 Spectrometer

At the time of the E791 run, the spectrometer consisted of: 23 planes of Silicon Micro-strip Detectors (SMDs) - 6 upstream of the secondary target foils for beam tracking and 17 downstream for primary and secondary particle tracking, Proportional Wire Counters (PWCs) - 8 upstream of the secondary target foils and downstream of the upstream SMDs for beam tracking and 2 downstream of the downstream SMDs for primary and secondary particle tracking, 4 drift chambers (DC1-DC4) for tracking throughout the detector, two analysis magnets (M1 and M2) for determination of charged secondary particle momenta, 2 Cherenkov counters (C1 and C2) for charged particle identification (PID), a segmented liquid ionization calorimeter (SLIC) for electron identification, a hadronic calorimeter (hadrometer), and finally a Muon system consisting of a 102 cm thick wall of steel and two walls of plastic scintillating paddles connected to photo-multiplier tubes (PMTs), one to determine the x-position and one to determine the y-position of the muons which pass through the steel (other particles should be stopped within the steel).

16

5.2 The E791 Data Set

As with the E791 detector, a more complete description of the E791 data set and the data reduction procedures used in analyzing the data can be found in [Witchey, pg 42]; a brief description of the E791 data set and its reduction follows.

The E791 data set contains over 20×10^9 triggers recorded on over 24,000 8mm video-tapes from which more than 100,000 charm events have been fully reconstructed. The 'raw' data set, *i.e.* data actually recorded at beam-time, was reformatted and reduced in a reconstruction and filtering procedure which produced a set of 3×10^9 events on approximately 8,000 Data Strip Tapes (DSTs). These DSTs were the starting basis for all analyses performed by the E791 collaboration. The reconstruction of this mammoth 'raw' data set was accomplished using a number of computer 'farms', large numbers of client computers integrated by a server computer using Parallel Virtual Machine (PVM) software. These farms were located at Kansas State University, University of Mississippi, Centro Brasileiro de Pesquisas Fisicas, and Fermilab.

Reconstruction consisted of first converting the 32-bit integers corresponding to detector hits in the SMDs and DCs for both the beam, primary and secondary particles into three-dimensional tracks passing through the
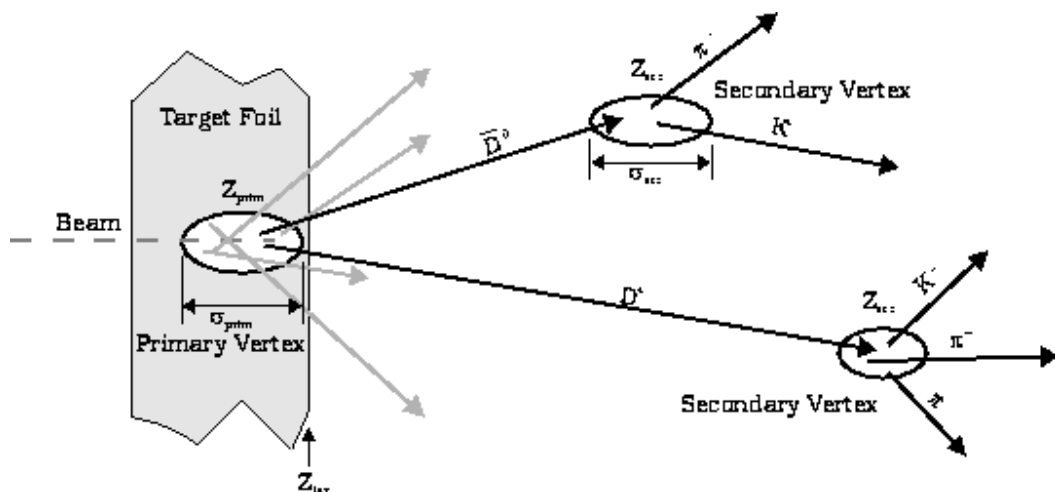

Figure 5.4 - Primary and Secondary Vertices

17

spectrometer. These tracks were then assembled into primary vertices, where at least two downstream tracks intersected with a beam track near one of the secondary target foils. Secondary vertices were formed from downstream tracks which intersected near a primary vertex. In both cases, once a vertex was identified, additional tracks were added to the vertex until the χ^2/dof (*i.e.* the chi squared per degree of freedom: the standard merit of fit) calculated from the tracks' impact parameters rose above ten. Each primary vertex and all resulting secondary vertices are then called an 'event', see *Figure 5.4*. Events which did not pass certain minimal cuts on the basis of this preliminary reconstruction were filtered out of the data set and only those which did pass were fully reconstructed by adding Cherenkov particle identification (PID) and calorimetry information.

These DSTs were then run through a number of 'strips' - each strip reducing the data set considerably, and focusing the remaining data on particular decay modes or events. This process of sequential stripping eliminated events on the basis of increasingly more demanding 'cuts', *i.e.* by requiring that various variables describing the event had values greater than or lower than or equal to the cut. Depending on the final analysis being performed, the reconstructed data would be run through a strip, sub-strip, a micro-strip, and even a nano-strip.

For the $f_0(980)$ analysis presented here, a $D_S^\pm$ FCNC nano-strip data set developed by N. Witchey for his doctoral dissertation [Witchey, pg 49] was used. It consists of approximately 2×10^6 events on 4 tapes.

Chapter 6 - Data Analysis

6.1 Signal Identification

The data used for this analysis comprises approximately two-thirds of one tenth of one percent of the reconstructed data set for E791. Every event in the $D_S^\pm$ FCNC data set has at least one vertex for which every variable listed in

variable	type/units	cut	strip	sub	micro	nano	description
tracks	number	=	3	3	3	3	# of tracks in vertex
|q|	charge	=	1	1	1	1	charge of primary vertex
sdz	number	>			8	10	vertex separation
tau	psec	<	5		3	2	life time
xyzvtx	cm	<	-.35	-.35	-.35	-.35	vertex position
dca	cm	<	.01	.01	.01	.01	distance close approach
P_t	GeV	<		.50	.35	.35	transverse momentum
|p|	GeV	<	500	500	500	500	total momentum
pp	GeV	<	500	500	500	500	each track's momentum
jcatsg	number	$\geq$	3	3	3	3	each track's category
xis	number	$\leq$		6.5	6.5	5.0	χ^2 of each track
itpok	logic	=		TRUE	TRUE	TRUE	vertex quality

Table 6.1 - $D_S^\pm$ FCNC and $f_0(980)$ Cuts

Table 6.1 satisfies the relation expressed between the *variable*, *cut*, and the value of the variable listed in the *nano* column (the other three levels of stripping are also presented to show how the cuts were successively tightened). Blank cells indicate that that particular variable was not cut on at that level of stripping.

Some of the cut variable descriptions are fairly obvious; the less obvious are defined as follows:

sdz	A measure of the separation of the primary and secondary vertices; see *Figure 5.4*. In terms of the quantities in that *Figure*, sdz is defined as:

$$sdz = \frac{z_{\sec} - z_{prim}}{\sqrt{\sigma_{prim}^2 + \sigma_{\sec}^2}} \qquad (6.1)$$

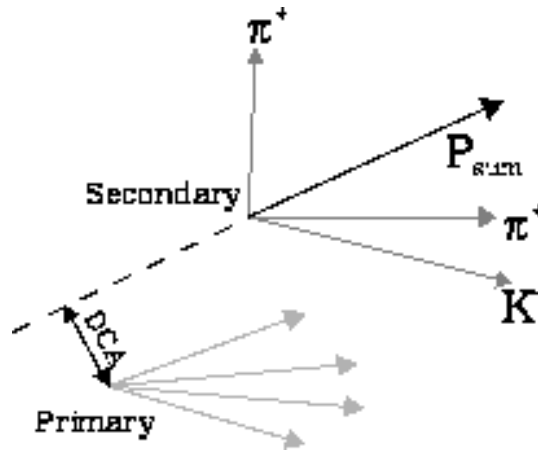|	
dca	(Distance of Closest Approach) A measure of how well the momentum of the reconstructed charm particle extrapolated to the primary vertex. It was defined by the vector sum of the visible daughters' momenta, see *Figure 6.1*:

Figure 6.1 - Distance of Closest Approach

|	
P_t	Charm decays including neutral daughters cannot be fully reconstructed - the 'missing' mass of the neutral daughter can make these primary vertices look like background because of resulting mass mis-assignment or mass-peak smearing. In such vertices, the sum of the momentum vectors of all visible daughters do not point along the momentum vector of the decaying charm particle. The difference between the two is P_t and is represented in *Figure 6.2*.
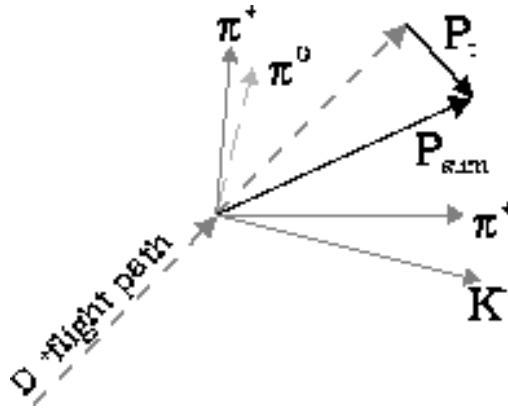
Figure 6.2 - P_t

jcatsg   A number assigned to each track based on the detectors which recorded hits for that track: these numbers are given in *Table 6.2.*

Category	Detectors Hit
0	SMDs only, No DCs
1	D1
3	D1, D2
7	D1, D2, D3
15	D1, D2, D3, D4

Table 6.2 - *jcatsg* Track Category

itpok   A logical variable which indicates the quality of a vertex's reconstruction - it is true if all of the following conditions were met for a particle vertex:

- $0 < $(number of tracks in vertex)≤ 36

- All tracks in vertex had jcatg≥ 3

- All tracks in vertex had charge$\neq 0$

- The momentum of all particles in a vertex is ≥ 0

- All tracks in vertex had $\chi^2/dof \leq 6.5$

21

From the $D_S^\pm$ FCNC set of events, each of which had at least one vertex which passed the cuts outlined above, signal events were selected on the following basis. For each three-track vertex with a charge Q=±1, the maximal Cherenkov probability of each track was used to identify each particle as an electron, muon, pion, kaon, or proton. Only those events were kept where, of the three particles, one was a pion, and the other two were kaons of opposite charge; this is the Cabibbo-favored decay; see **Chapter 4.2**. All other events were considered background. This selection process is exemplified by a

Vertex(Event)#22(20) is signal#1			
charge:	-1.0	1.0	1.0
elec:	0.0000	0.0195	0.0039
muon:	0.0000	0.0117	0.0039
pion:	0.1289	0.8086	0.3242
kaon:	0.6523	0.1211	0.5039
proton:	0.2188	0.0391	0.1680
greatest:	0.6523	0.8086	0.5039
type:	4	3	4
potential Ds: (k-pi+k+/k+k-)			
invariant mass: 1.9692/0.9914			

Table 6.4 - Signal Event ID

Vertex(Event)#19(17) is background#7			
charge:	1.0	-1.0	-1.0
elec:	0.0039	0.0000	0.0000
muon:	0.1406	0.0938	0.0039
pion:	0.5352	0.8438	0.9766
kaon:	0.2422	0.0469	0.0117
proton:	0.0820	0.0156	0.0039
greatest:	0.5352	0.8438	0.9766
type:	3	3	3
background: (pi+pi-pi+)			
invariant mass: 1.9692/.09914			

Table 6.3 - Background Event ID

fragment of analysis code output; see *Tables 6.3* and *6.4*.

This selection routine is entirely dependent on the Cherenkov Counters which are not perfect, and as a result, there is a certain amount of misidentification.
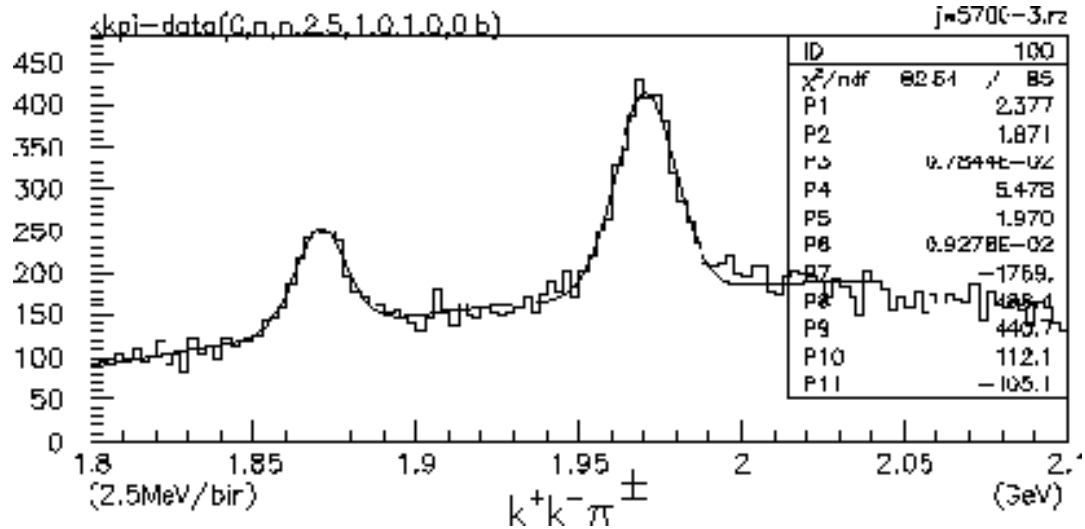

Figure 6.3 - $D^{\pm}$ and $D_S^{\pm}$ with $D^{\pm}$ Reflection

This misidentification can be seen immediately by plotting the invariant mass of the $K^+K^-\pi^{\pm}$ in the region about the $D_S^{\pm}$, *i.e.* 1.7-2.05 GeV, see *Figure 6.3*. Notice that the fit (see **Chapter 6.4** for a full description of the fit) in *Figure 6.3*, is not excellent: χ^2/dof=1.25 - it is a little too high between the $D^{\pm}$ and $D_S^{\pm}$ peaks.

The Cabibbo-favored decay, $D^{\pm} \to K^{\mp}\pi^{\pm}\pi^{\pm}$ can explain this, however, if one considers the possibility that one of the π^{-} has been misidentified as a K^{-}, thus making the event look as though it was the signal event $D_S^{\pm} \to K^{+}K^{-}\pi^{\pm}$. If the 'off-sign' kaon, *i.e.* the daughter opposite in charge to the $D^{\pm}$, is forced to have a the mass of a pion, and then the invariant mass of the three particles is plotted, *Figure 6.4* results. The peak in the vicinity of the $D^{\pm}$, *i.e.* 1869 MeV, means that indeed, some of the events identified in *Figure 6.3* as $K^{+}K^{-}\pi^{\pm}$, were, in fact, $K^{\mp}\pi^{-}\pi^{-}$ from a $D^{\pm}$. That this peak is much wider than the $D^{\pm}$ found in the $K^{+}K^{-}\pi^{\pm}$ plot, ~7.5 MeV (*P3*), indicates that the misidentification is a small effect. Even so, the misidentified $K^{\mp}\pi^{-}\pi^{-}$ appear on the high side of the $D_S^{\pm}$ because the pion, whose mass is only 139.6 MeV, has been misidentified a kaon, whose mass is 494 MeV.
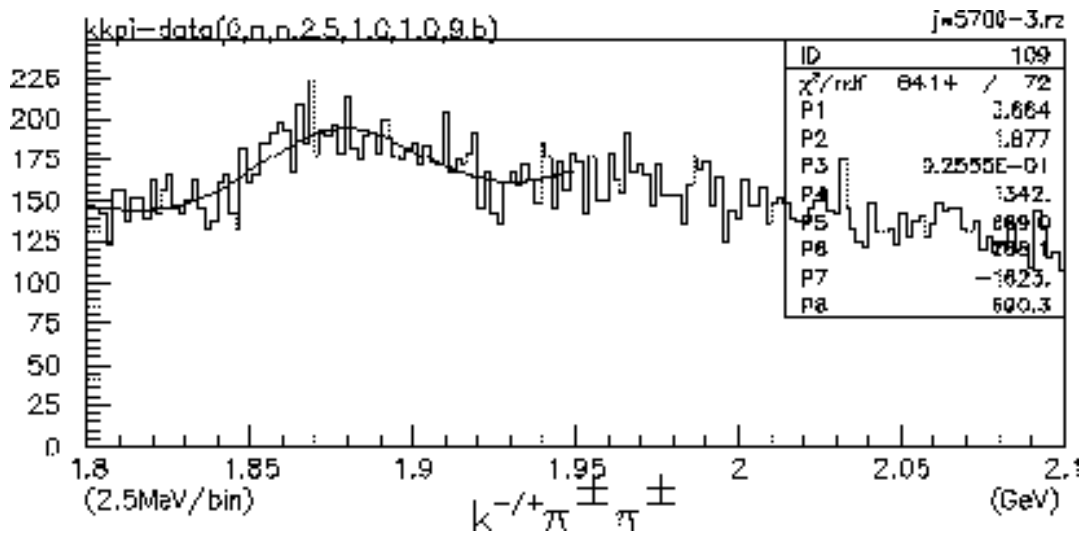

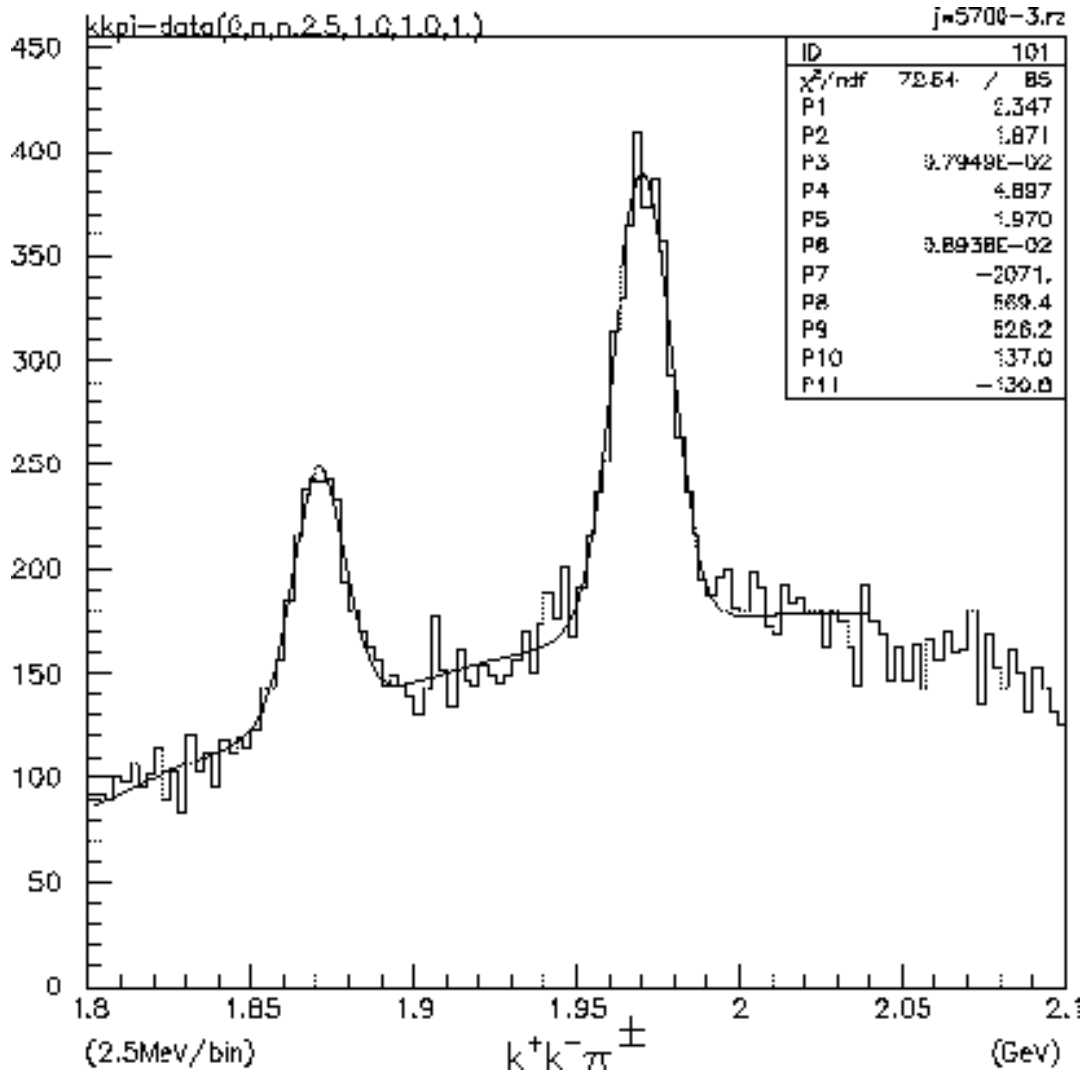Figure 6.4 - $D^{\pm}$ from $K^{\mp}\pi^{\pm}\pi^{\pm}$ Misidentified as $K^{+}K^{-}\pi^{\pm}$

Figure 6.5 - $D^{\pm}$ and $D_S^{\pm}$ without $D^{\pm}$ Reflection

To correct for this misidentification, those events whose invariant $K^{\mp}\pi^{\pm}\pi^{\pm}$ mass fall in the range (1870±8)MeV (*P2±P3)* are not plotted in the $K^{+}K^{-}\pi^{\pm}$ mass plot and *Figure 6.5* results*.*

The $D_S^{\pm}$ is still sitting on a background of ~80 $K^{+}K^{-}\pi^{\pm}$ events per bin - what is this background? There are other primary particles whose decay daughters are being misidentified, but the $D^{\pm}$ is the only significant source of this kind of background. Some of it is $K^{+}K^{-}\pi^{\pm}$ where one or more of the particles are not the daughters of the *same* primary particle. For instance, the

normalizing mode in this work is $D_S^\pm \to \left(\phi \to K^+ K^-\right)\pi^\pm$. It is possible, however, that a ϕ, which later decays into a K⁺K⁻ pair, and pion are produced independently, and which together, just happen to have an invariant mass close to that of a $D_S^\pm$. In this example, the $K^+ K^-$ are daughters of the same parent, but of course, any two of the three particles might be might be daughters of the same parent while the other is not, and it is possible that all three particles were created independently.

In E791, the only particles identified directly are electrons, muons, pions, kaons, and protons - all other particles are inferred by means of mass plots and fits to these plots which have central mass values and widths which are known to correspond to other particles. All intermediate states, *e.g.* the $D_S^\pm$ and ϕ in the decay $D_S^\pm \to \left(\phi \to K^+ K^-\right)\pi^\pm$, are merely inferred, while the final state of $K^+ K^- \pi^\pm$ is 'detected'. For this reason, treatment of non-resonant $K^+ K^- \pi^\pm$ will be discussed in **Chapter 6.4.**

Finally, these methods of eliminating background are somewhat cosmetic - the vast majority of background is eliminated by the cuts applied to generate the data set in the first place. The cuts were optimized to maximize the ratio:

$$\frac{Signal}{\sqrt{Background}} \equiv \frac{S}{\sqrt{B}}$$

There will always be a certain amount of background, but if the background is very well known, then it becomes unimportant. When the background is large,

Level	$S/\sqrt{B}$	# of Tapes	# of Events
raw	???	24,000	2×10^{10}
strip	≪1	2,400	1×10^{9}
sub	≈1	290	1×10^{8}
micro	≥1	30	1×10^{7}
nano	≈2	4	2×10^{6}

Table 6.5 - $S/\sqrt{B}$ for Each Level of Stripping

bin by bin, the uncertainty in the background can be well approximated by the square root of the number of background events, bin by bin. Thus, when the background is large, maximizing $S/\sqrt{B}$ has the effect of minimizing the uncertainty in the background. *Table 6.5* shows the $S/\sqrt{B}$ at each level of stripping, and the number of events and tapes at each level.

For the $D_S^{\pm}$ FCNC data set, the two single most important cuts were the *sdz* and *tau* cuts - *sdz* eliminated almost all events that were not charm, and *tau* drastically reduced the number of the longer-lived charm events, *e.g.* $D^{\pm}$. For a more detailed discussion of the signal to background ratio, see [Witchey, pg 67].

6.3 Fitting

As a note on the presentation of all invariant mass plots in this work, all mass spectra are fit in the following fashion: the first three parameters (*P1-P3*) of each plot describe the first peak, and if there is a second peak, then second set of three parameters (*P4-P6*) describe the second peak. For $D^{\pm}$ and $D_S^{\pm}$ peaks (both Monte Carlo and data) a gaussian fit was used:

$$\frac{A}{\sigma\sqrt{2\pi}} e^{-\frac{\left(m_0 - m\right)^2}{2\sigma^2}}$$

P1(P4)=A   *P2(P5)=m_0*   *P3(P6)=σ*

Normalized in this fashion, (*P1/binwidth*)=(# of counts under the peak).

For ϕ peaks, a Breit-Wigner peak was used:

$$\frac{B}{\pi\left(\Gamma/2\right)} \frac{\left(\Gamma/2\right)^2}{(m_0 - m)^2 + \left(\Gamma/2\right)^2}$$

P1(P4)=B   *P2(P5)=m_0*   *P3(P6)=Γ*

Where again, normalized in this fashion, (*P1/binwidth*)=(# of counts under the peak).   For the $f_0(980)$, the WA76 parameterization (see **Chapter 4.1**) was used:

$$\left(\Gamma_K + D\Gamma_\pi\right)\frac{(C*3.06055)}{\left(m_0^2 - m^2\right)^2 + m_0^2\left(\Gamma_k + \Gamma_\pi\right)^2} \tag{6.1}$$

$$P1=C \qquad\qquad P2=m_0 \qquad\qquad P3=D$$

In this case, the integral over this function is not analytic, and the factor of 3.06055 is introduced to normalize the function to 1 over the mass range 280MeV (the $\pi\pi$ threshold) to 1680MeV - this range was chosen to be approximately symmetric about the f_0(980)'s central mass value. As a result, (*P1/binwidth*)=(# of counts under the peak). The third parameter was included so that the pion decay channel could be 'closed off' to examine the line-shape arising from the two channels independently. In most fits, D=0 with no possibility of variation.

All fits to KKπ invariant mass plots include a 4th order polynomial background:

$$P4(P7)+P5(P8)m+P6(P9)m^2+P7(P10)m^3+P8(P11)m^4.$$

On the other hand, all K^+K^- mass plots include a background which is assumed *a priori* to have a cutoff at twice the rest mass of a $K^\pm$ (m_0=987.4 *MeV*), and so the function:

$$E(m-m_0)^F e^{-G(m-m_0)}$$

$$P1(P4)=E \qquad\qquad P2(P5)=F \qquad\qquad P3(P6)=G$$

is used - it rises rapidly after threshold, but the then dies out as *(m-m$_0$)* grows large.

Furthermore, where mass plots have large numbers of empty bins, a log-likelihood fit is used. In this case, χ^2/dof is no valid a s a merit of fit, and is not reported. Only when a simple χ^2 fit is possible, *i.e.* when there are few or no empty bins, is the χ^2/dof reported.

6.3 Monte Carlo Efficiencies

To calculate the efficiency of the detector for the two modes of interest, Monte Carlo simulations were run for each mode. For the normalizing mode $D_S^{\pm} \rightarrow \left(\phi \rightarrow K^+ K^- \right) \pi^{\pm}$, the Monte Carlo was required to produce a $D_S^{\pm}$, which was required to decay into a ϕ. Likewise, for the $D_S^{\pm} \rightarrow \left(f_0(980) \rightarrow K^+ K^- \right) \pi^{\pm}$ mode, the required $D_S^{\pm}$ was forced to decay into the $f_0(980)$. In both cases, the intermediate particle, the ϕ and $f_0(980)$, were then forced to decay to $K^+ K^-$. The efficiencies, ε_{ϕ} and ε_{f_0}, are then defined to be the number of events, $D_S^{\pm} \rightarrow \phi \pi^{\pm}$ and $D_S^{\pm} \rightarrow f_0(980) \pi^{\pm}$, respectively, 'detected' after generation and reconstruction, divided by the number of events (of each type) generated. In both cases, the Monte Carlo data is run through the same analysis code used on the actual data, so that 'apples' are compared with 'apples'.
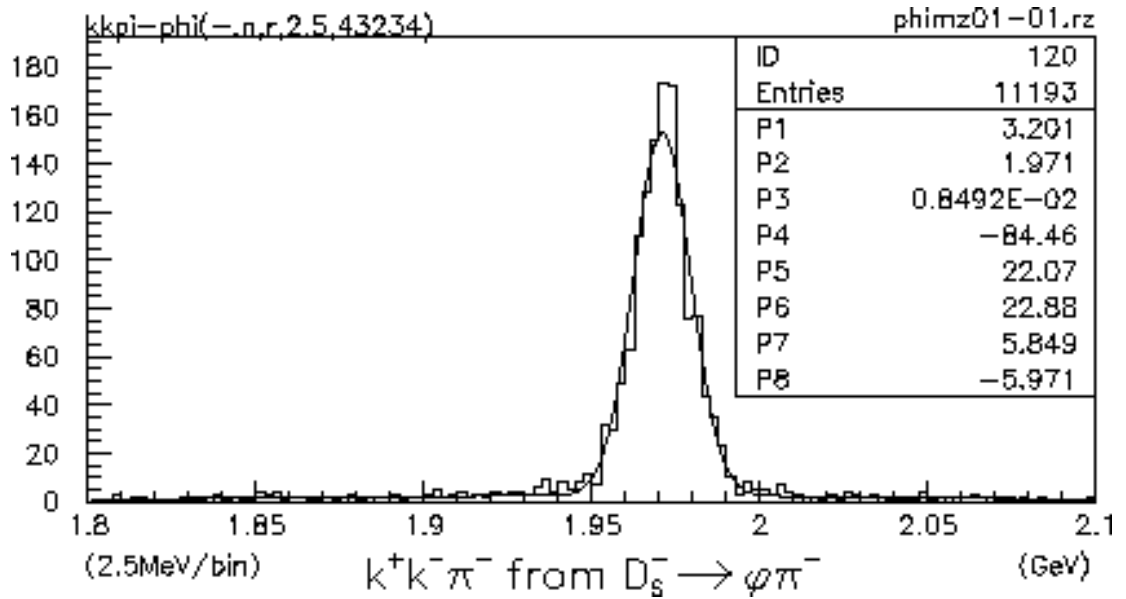
Figure 6.6a - Monte Carlo $K^+K^-\pi^-$ for $D_S^- \to \phi\pi^-$

Turning to the Monte Carlo data itself, *Figure 6.4* shows the $D_S^\pm \to (\phi \to K^+K^-)\pi^\pm$ Monte Carlo data. 125,000 events were generated for each charge state. The finite mass resolution of the spectrometer yields a full-width-at-half-max (FWHM) of ~19 MeV.

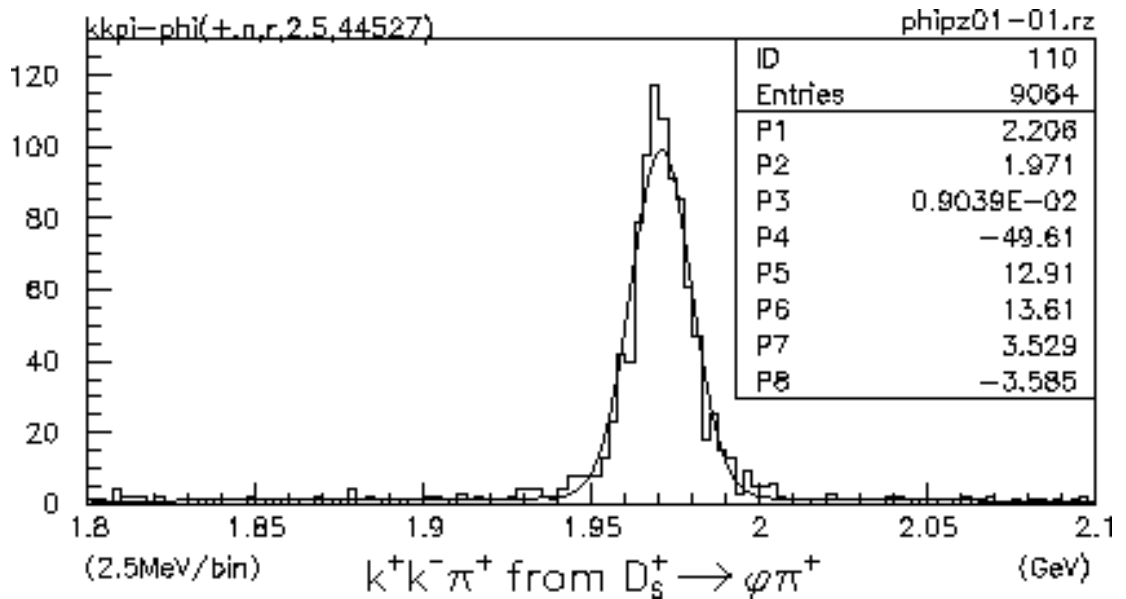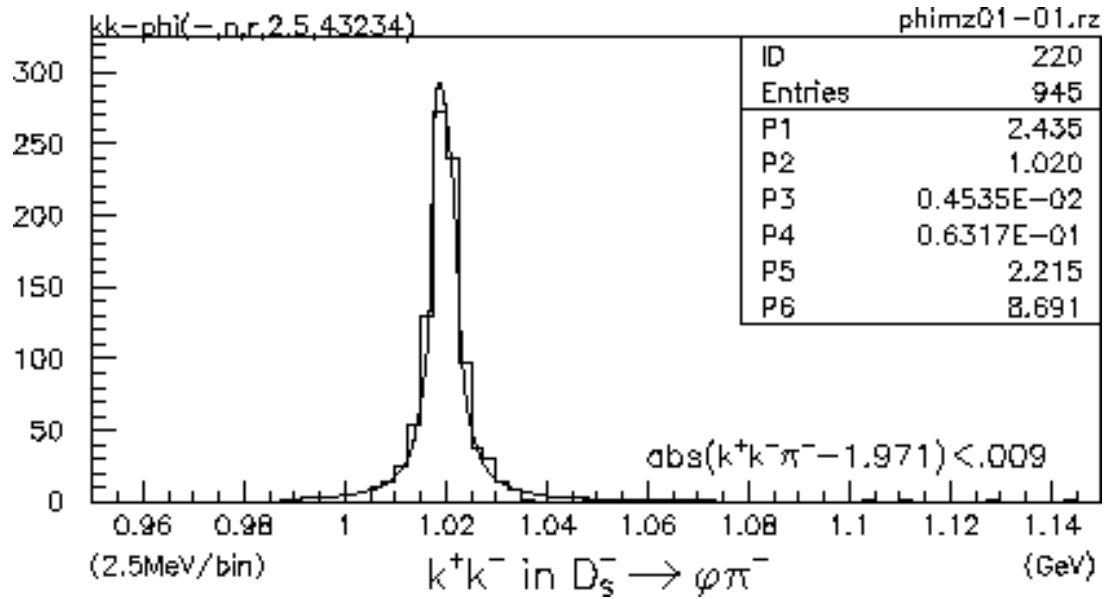Figure 6.6b - Monte Carlo $K^+K^-\pi^+$ for $D_S^+ \to \phi\pi^+$

Figure 6.7a - Monte Carlo K^+K^- for $D_S^- \to \phi\pi^-$

The $D_S^\pm \to \phi\pi^\pm$ signal is then found by plotting the K^+K^- invariant mass from a region of 18 MeV centered about the central mass value of the $D_S^\pm$, 1971 MeV (from the fit on *Figures 6.4a* and *6.4b*), see *Figures 6.5a* and *6.5b*.
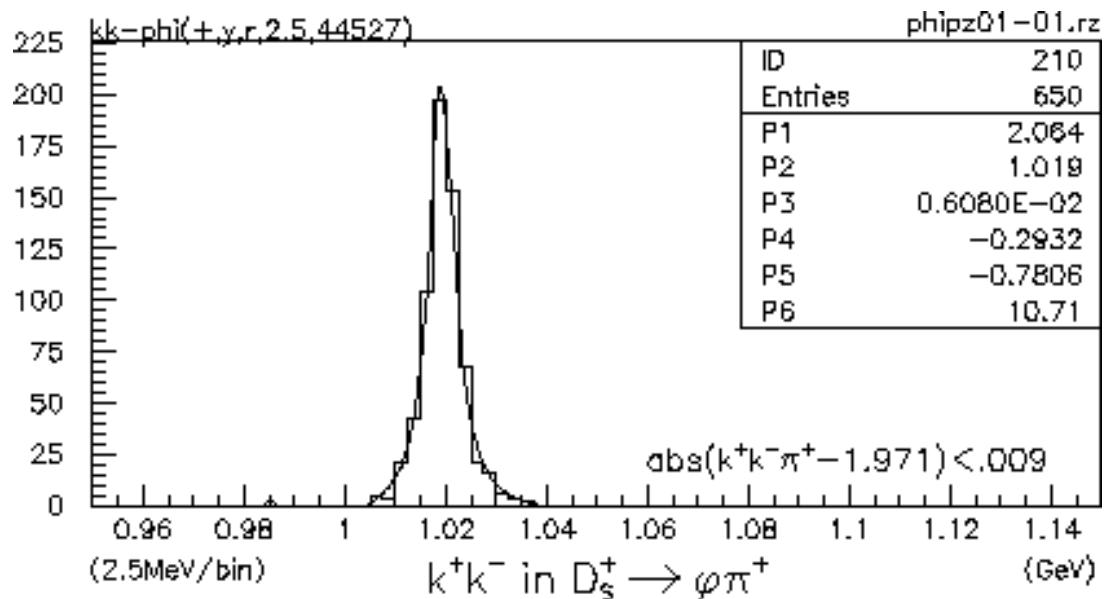
Figure 6.7b - Monte Carlo K^+K^- for $D_S^+ \to \phi\pi^+$

	$D_S^- \to \left(\phi \to K^+K^-\right)\pi^-$		$D_S^+ \to \left(\phi \to K^+K^-\right)\pi^+$	
Decay:	Number of:	Efficiency of:	Number of:	Efficiency of:
$D_S^\pm \to K^+K^-\pi^\pm$	1281±38	0.0102±0.0003	882±31	0.0071±0.0003
$D_S^\pm \to \phi\pi^\pm$	947±42	0.0078±0.0003	825±55	0.0066±0.0004
$\varepsilon_\phi \equiv eff\left(D_S^\pm \to \phi\pi^\pm\right) = \dfrac{\left(0.0078 \pm 0.0003\right) \pm \left(0.0066 \pm 0.0004\right)}{2} = 0.0072 \pm 0.0003$				

Table 6.6 - Numbers and Efficiencies of $D_S^\pm \to \phi\pi^\pm$

The number of events detected, and the efficiency of detection for $D_S^\pm \to \left(\phi \to K^+K^-\right)\pi^\pm$ are presented in *Table 6.6*.

For the $D_S^\pm \to \left(f_0(980) \to K^+K^-\right)\pi^\pm$, a similar procedure was followed. In order to generate the $f_0(980) \to K^+K^-$ decay, the Monte Carlo package used in this work, Pythia 5.7 and Jetset 7.4 [Sjostrand] required modification. When an $f_0(980)$ with a mass less than the rest mass of two $K^\pm$ was generated, an infinite loop would result, and the Monte Carlo would terminate gracefully after a certain number of such events. Though this number is under the control of the user, setting it to some obscenely large number is not a terribly elegant solution, so the mass generating subroutine of Jetset, ULMASS, was modified in the following manner.

First, in the routine which actually called the Jetset/Pythia package, a 'mass-lookup table' was created using the WA76 parameterization as a probability distribution function, and stored as a FORTRAN COMMON BLOCK. This function is given above *(6.1)* where the parameter D≡0.0. and the distribution is normalized to 1.0 as described above. Second, the ULMASS subroutine of Jetset was modified so that when it is was called to generate the mass of an $f_0(980)$, a random number [0,1] was generated, and this number was compared to the previously created WA76 parameterization probability distribution function and the $f_0(980)$ mass assigned appropriately. Since the

WA76 parameterization has a cutoff at twice the $K^{\pm}$ mass, see **Chapter 4.1**, no $f_0(980)$ were then generated with a mass less than this.
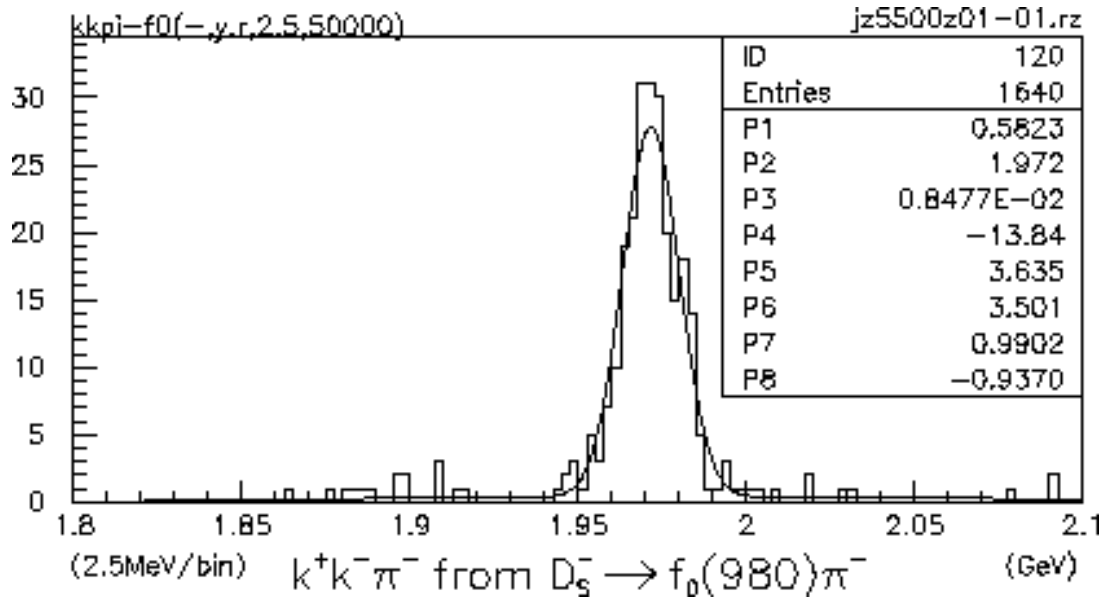
Figure 6.8a - $K^+K^-\pi^-$ for $D_S^- \to f_0(980)\pi^-$

Figure 6.8 shows the Monte Carlo generated $K^+K^-\pi^\pm$ for the $f_0(980)$ data. 50,000 events were generated for charge state of $D_s \to f_0(980)\pi$, as opposed to the 125,000 for $D_s \to \phi\pi$, and yet the D_s is clearly visible and well-defined in these two plots.
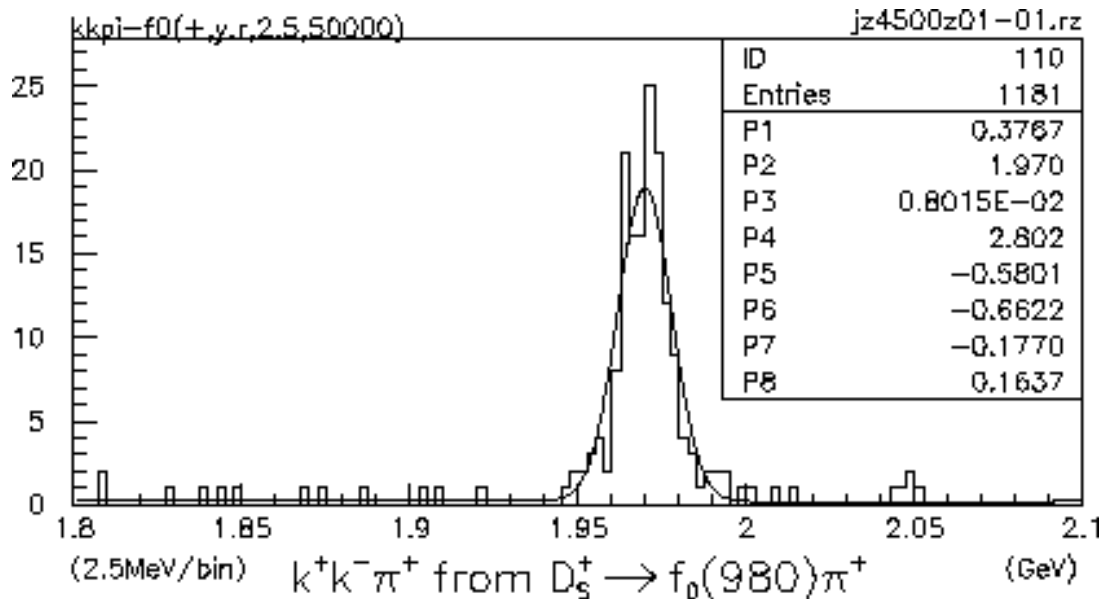

Figure 6.8a - $K^+K^-\pi^+$ for $D_S^\pm \to f_0(980)\pi^+$
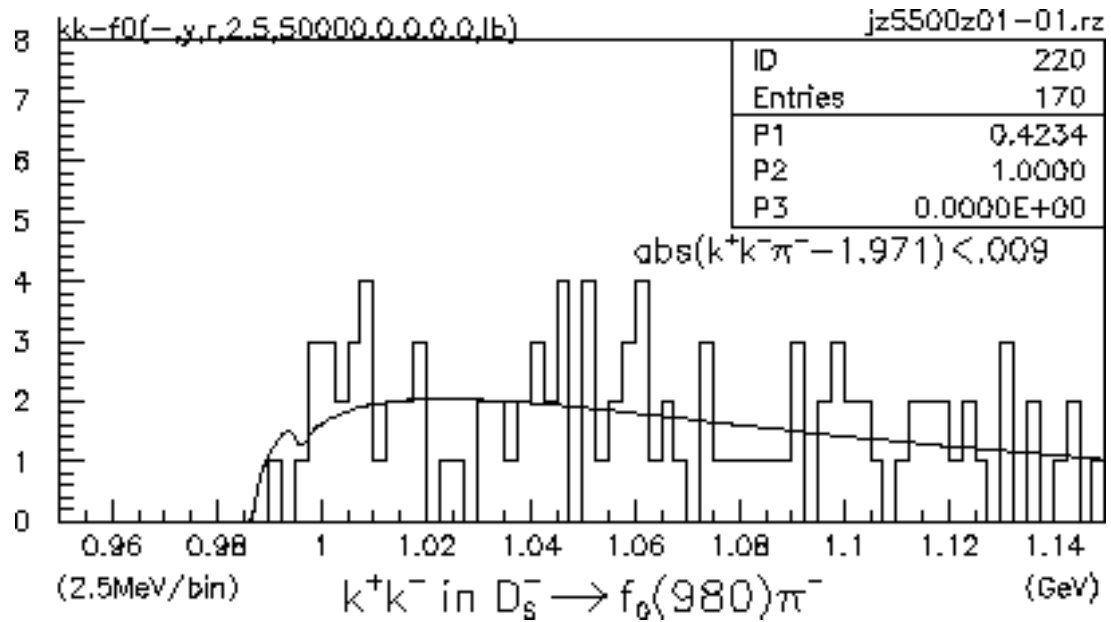
Figure 6.9a - K^+K^- for $D_S^- \rightarrow f_0(980)\pi^-$

Figure 6.9 shows the K⁺K⁻ for the f₀(980) Monte Carlo data. Again, the expected line shape is clearly evident, but the limited statistics of these Monte Carlo runs is evident from the empty bins. In both of these plots, *P1* and *P2*, the number of
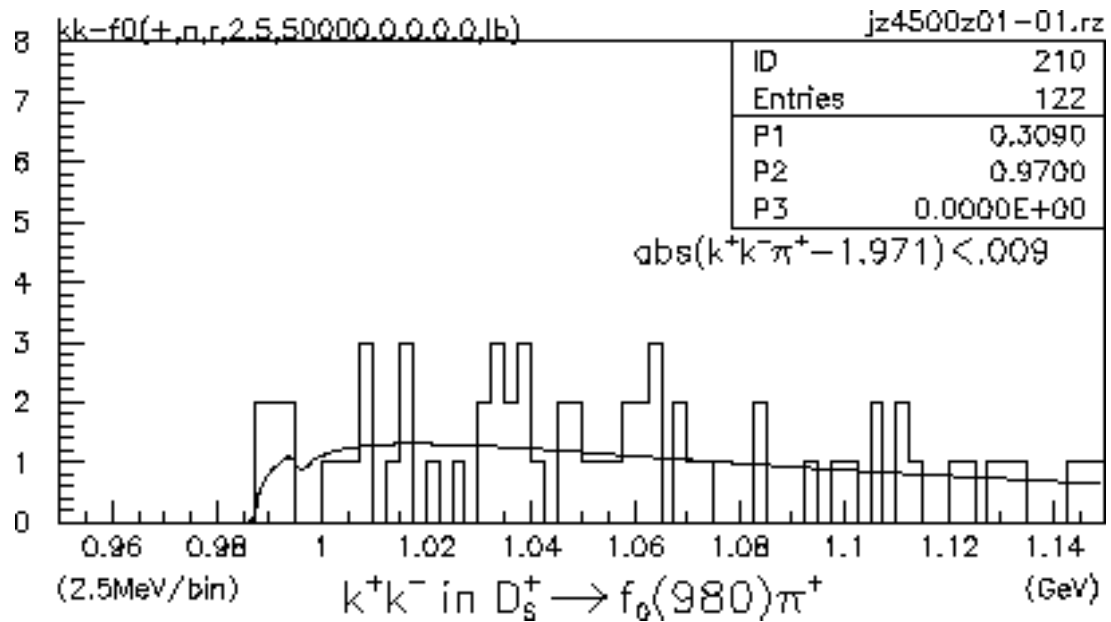

Figure 6.6a - K^+K^- for $D_S^\pm \rightarrow f_0(980)\pi^+$

$f_0(980)$ and the 'central mass' of the $f_0(980)$, respectively, were allowed to vary to examine the effects of the low statistics; only *P3* was not allowed to vary from 0.0.

The numbers and efficiencies for $D_S^\pm \to \left(f_0(980) \to K^+ K^-\right)\pi^\pm$ are presented

	$D_S^- \to \left(f_0(980) \to K^+ K^-\right)\pi^-$		$D_S^+ \to \left(f_0(980) \to K^+ K^-\right)\pi^+$	
Decay:	Number of:	Efficiency of:	Number of:	Efficiency of:
$D_S^\pm \to K^+ K^- \pi^\pm$	233±15	0.0047±0.0003	151±13	0.0030±0.0003
$D_S^\pm \to f_0(980)\pi^\pm$	169±18	0.0034±0.0003	124±21	0.0025±0.0004
$\varepsilon_{f_0} \equiv eff(D_S^\pm \to f_0(980)\pi^\pm) = \dfrac{(0.0034 \pm 0.003) + (0.0025 \pm 0.0004)}{2} = 0.0029 \pm 0.0003$				

Table 6.7 - Numbers and Efficiencies of $D_S^\pm \to f_0(980)\pi^\pm$

in *Table 6.7*.

6.4 Data

The $D_S^\pm$ FCNC $K^+K^-\pi^\pm$ mass plots are presented in *Figures 6.10a* and *6.10b*. These plots have already had the misidentified $D^\pm \rightarrow K^\mp \pi^\pm \pi^\pm$ eliminated, and the vertical lines indicate the $K^+K^-\pi^\pm$ mass-cut regions for identifying the $\phi\pi^\pm$ and $f_0(980)\pi^\pm$ resulting from the decay of a $D_S^\pm$ and those from other sources.
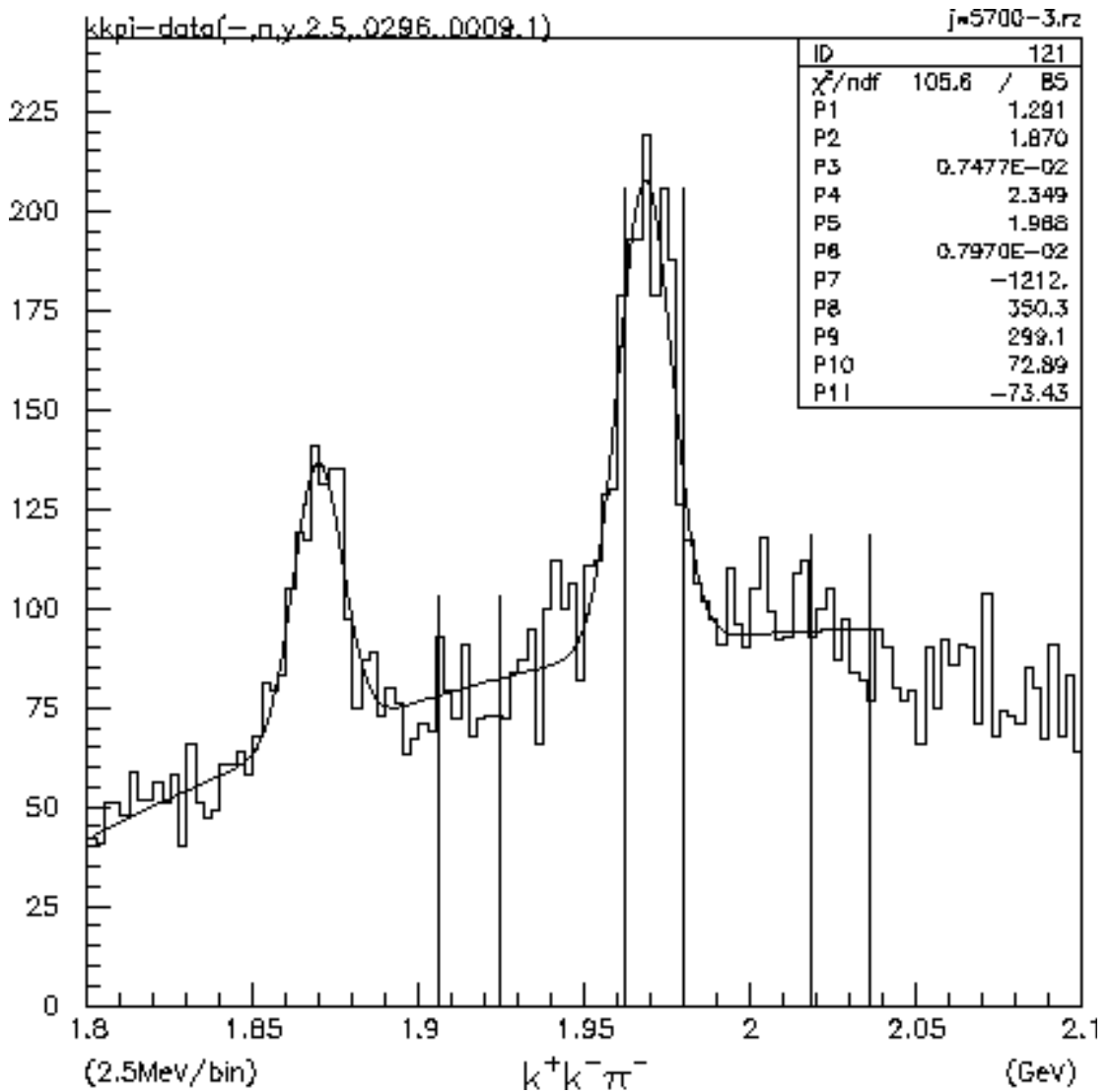

Figure 6.10a - $K^+K^-\pi^-$ from the D_S^- FCNC Data Set

The central region, $(1.962 \leq K^+K^-\pi^\pm \leq 1.980)$GeV, is designated as the $D_S^\pm$ signal region - only K^+K^- from this region are plotted and fit to determine the number of $D_S^\pm \to \phi\pi^\pm$ and $D_S^\pm \to f_0(980)\pi^\pm$ in the data. K^+K^- are plotted and fitted from the lower and upper regions or 'sidebands', $(1.906 \leq K^+K^-\pi^\pm \leq 1.924)$GeV and $(2.018 \leq K^+K^-\pi^\pm \leq 2.036)$GeV, respectively, to determine the number of $\phi\pi^\pm$ from sources other than $D_S^\pm$. The number of
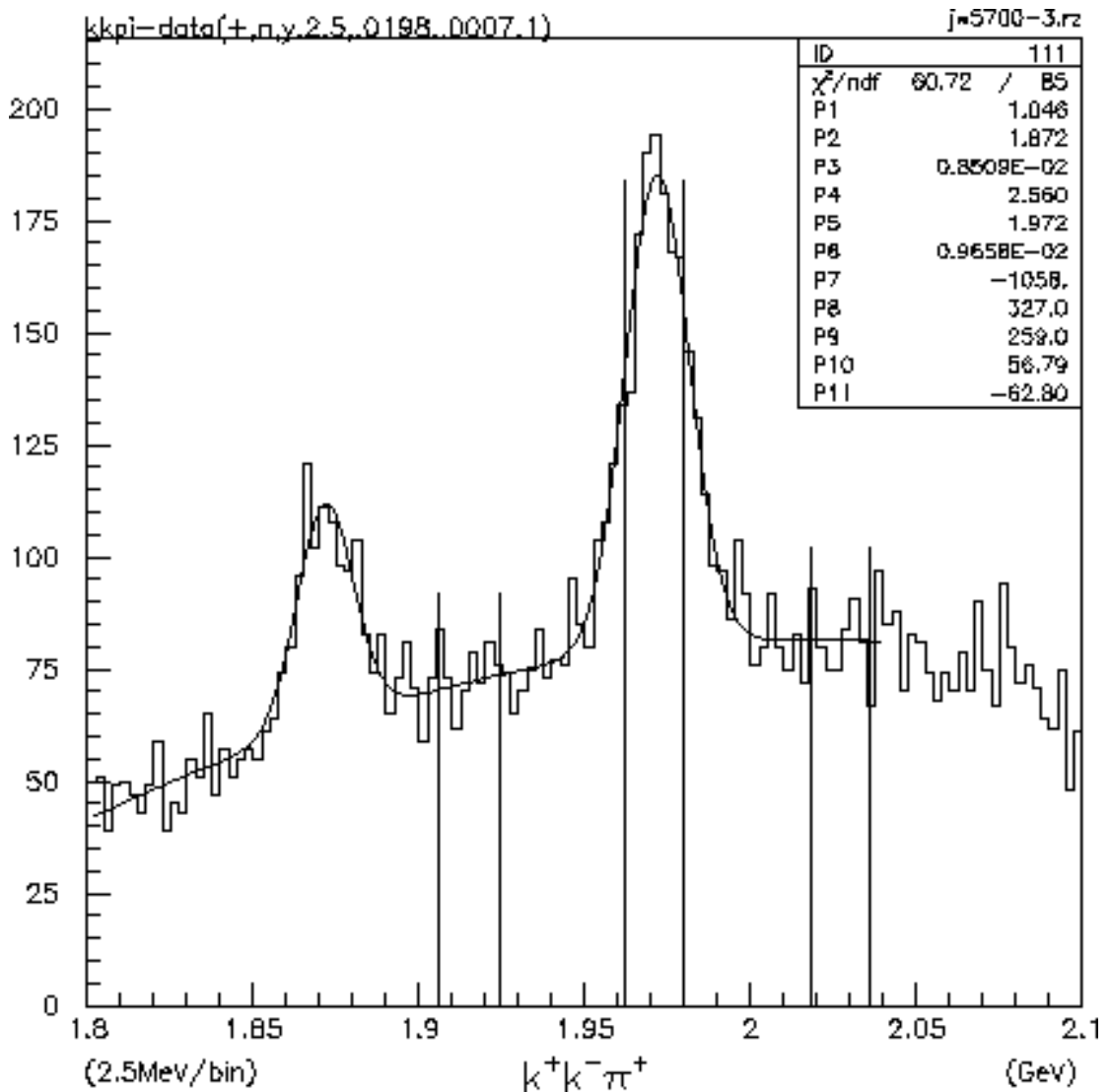

Figure 6.10b - $K^+K^-\pi^+$ from the D_S^+ FCNC Data Set

38

$f_0(980)$ from other sources is assumed to to be 0.0. The K^+K^- signal from the lower and upper sidebands, chosen well away from the $D_S^\pm$, are used to find the number of $\phi\pi^\pm$ from sources other then the $D_S^\pm$. Because the plots indicate that there could be at most one or two $f_0(980)$ in this region, the parameters for the $f_0(980)$ (*P1-P3*) areset to zero. The resulting parameters for the background (*P7-P9*) are then used for fitting the K^+K^- signal from the $D_S^\pm$ signal region.
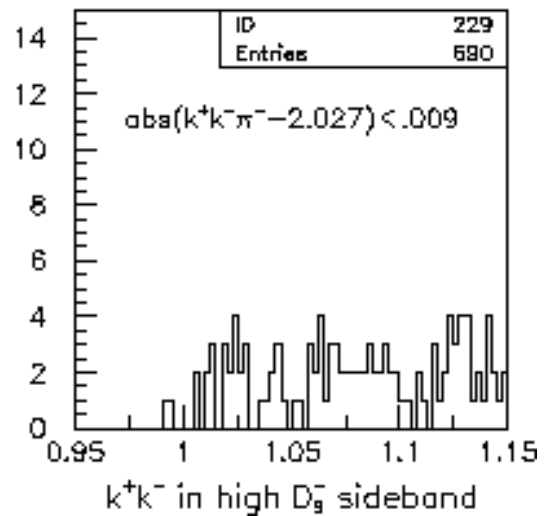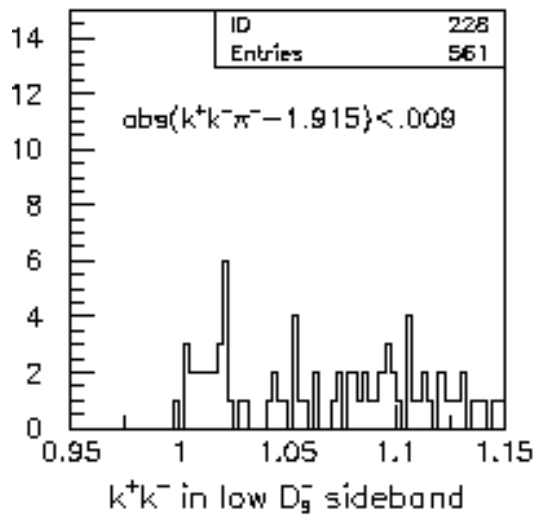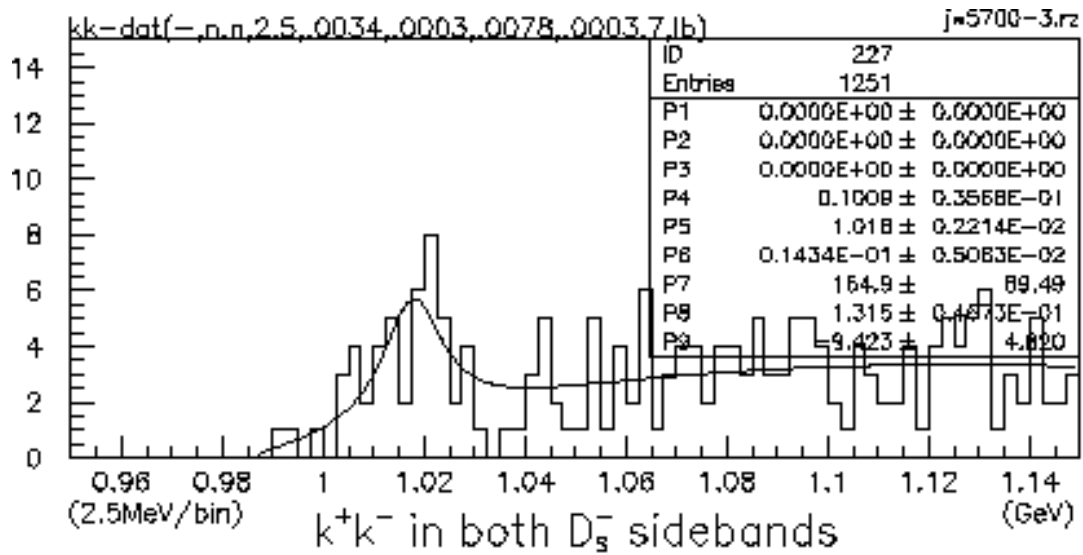

Figure 6.11a - K^+K^- from the Lower and Upper D_S^- Sidebands

Each sideband is the same width as the resonant signal region, so as to accumulate sufficient statistics for fitting purposes, and therefore the number of $\phi\pi^{\pm}$ found from the sum of the two sidebands is divided by two to normalize it to the $D_S^{\pm}$ signal region.
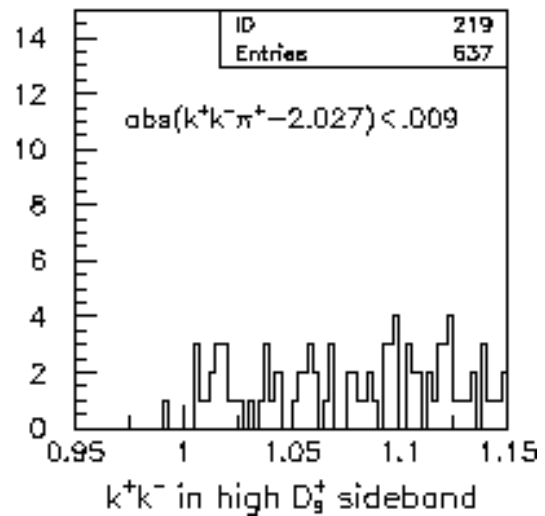

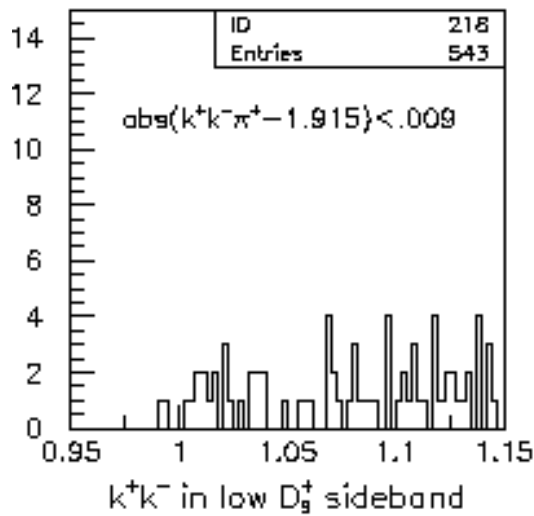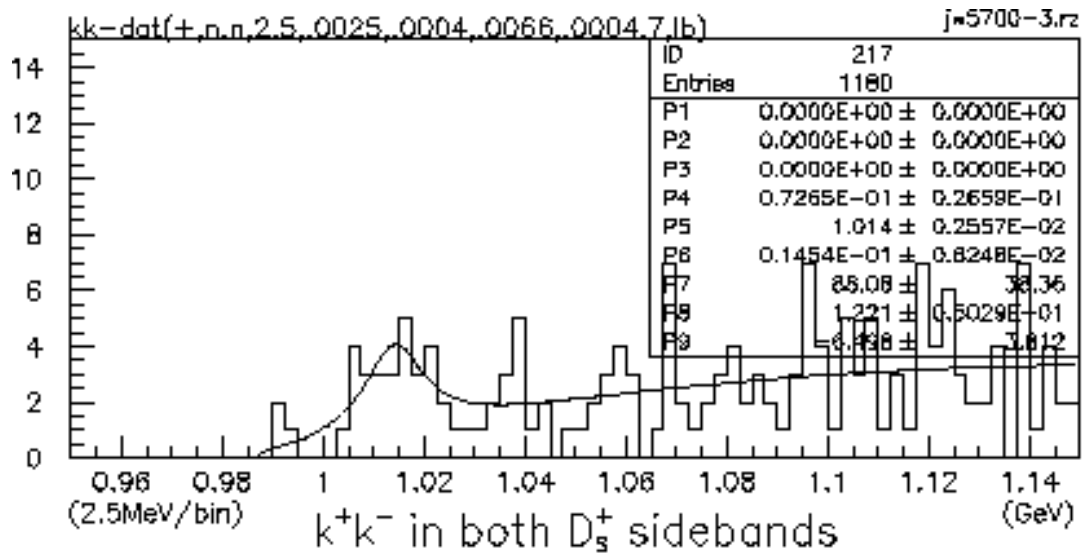
Figure 6.11b - K^+K^- from the Lower and Upper D_S^+ Sidebands

Finally, the K^+K^- from the $D_S^\pm$ signal region are plotted and fit. The number of $D_S^\pm \to \phi\pi^\pm$ will then be taken to be the number of $\phi \to K^+K^-$ from the $D_S^\pm$ signal region less the normalized sum of $D_S^\pm \to \phi\pi^\pm$ from the the sum of the lower and upper sidebands. The last two background parameters (*P8-P9*) from the sum of the lower and upper sideband regions, which describe the shape of the background, are held constant for the fit to the $D_S^\pm$ signal region.
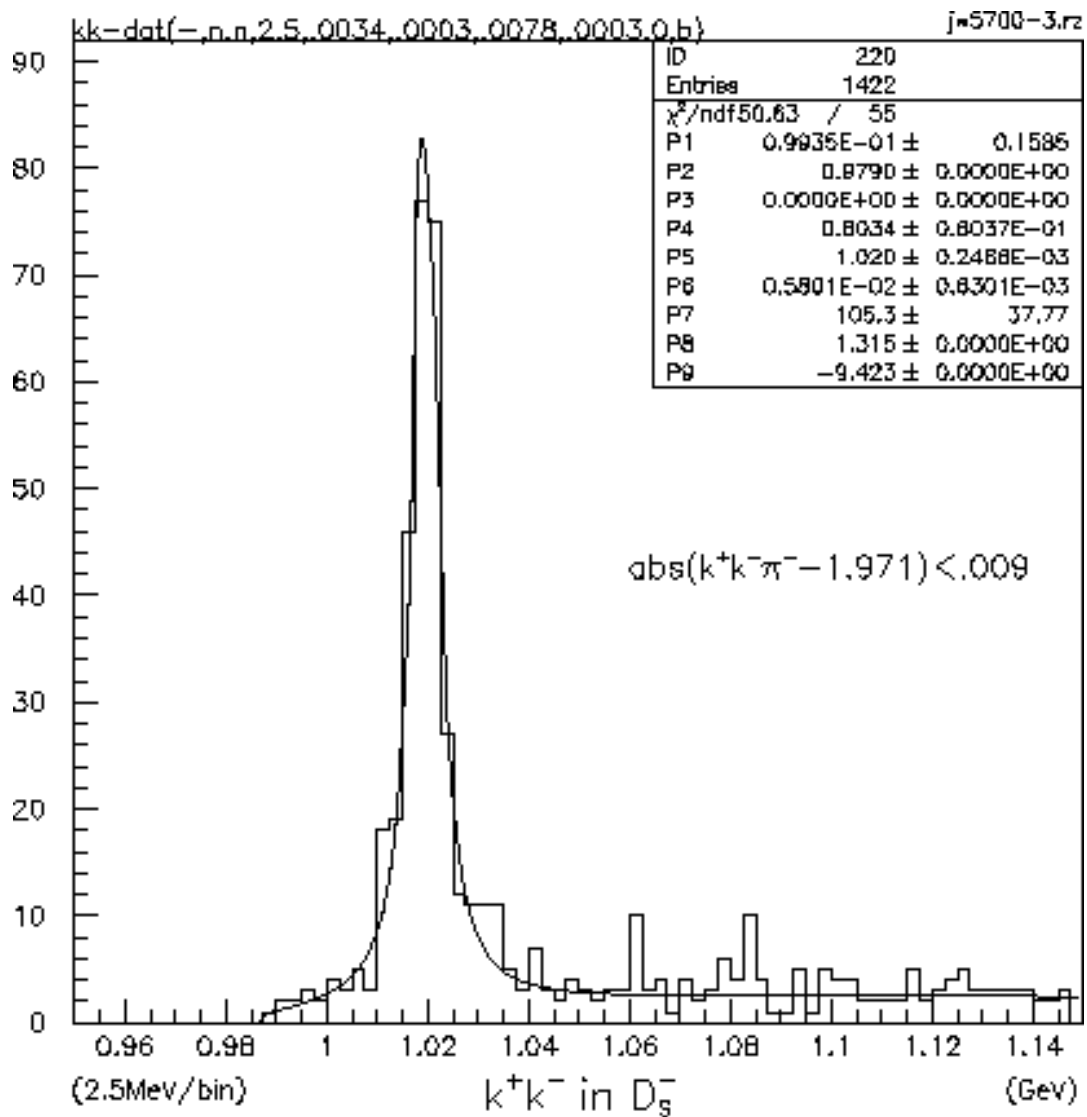

Figure 6.12a - K^+K^- from the D_S^- Signal Region

Only the first of the background parameters (*P7*), which is really nothing more than a scaling factor, is allowed to vary in the $D_S^\pm$ signal region fit of K^+K^- mass plot. The three parameters describing the $f_0(980)$ (*P1-P3*) then fit whatever 'rides above' this scaled background from the sideband fit. The number of $D_S^\pm \to f_0(980)\pi^\pm$ is then *P1/binwidth.*
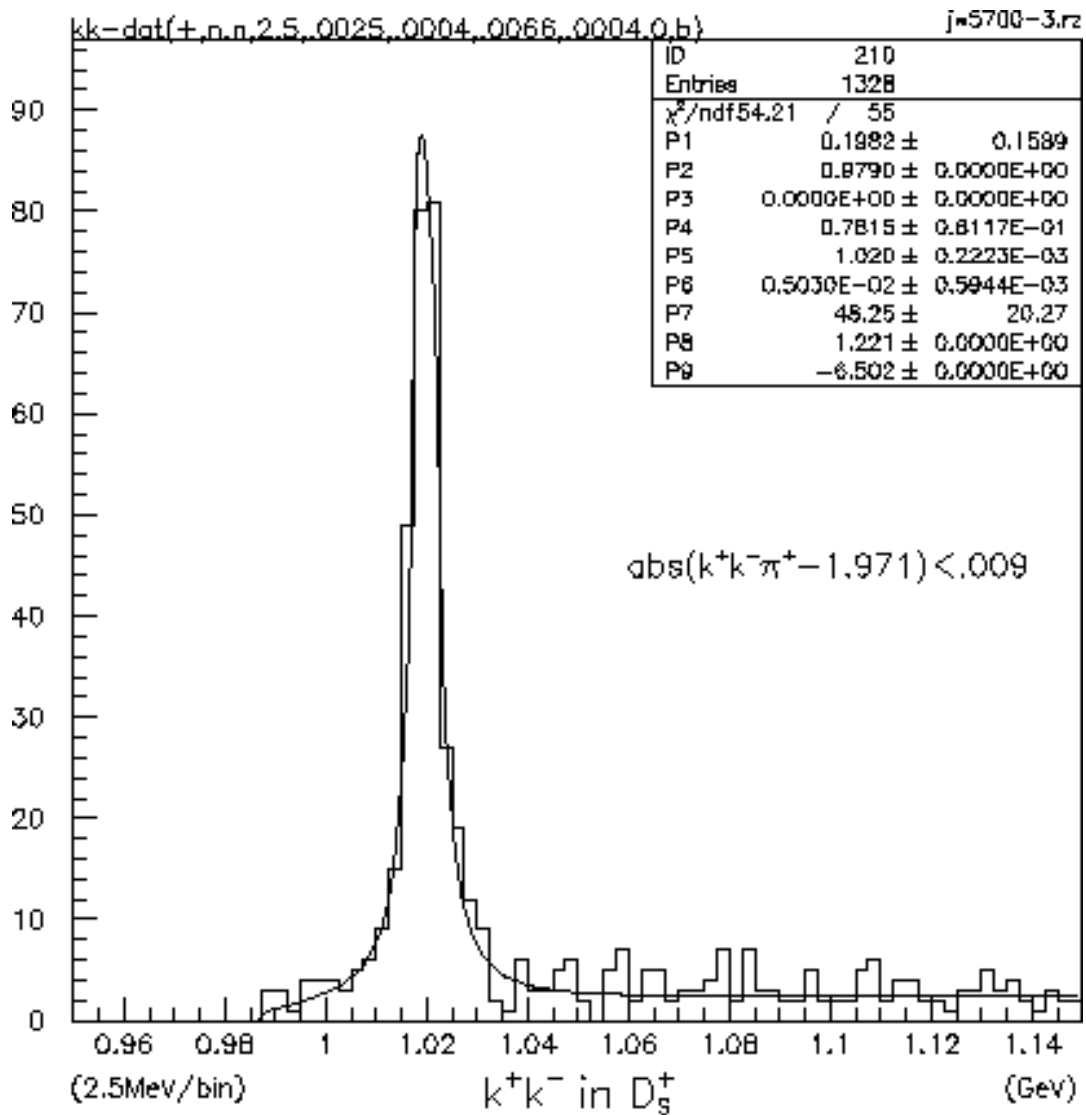
Figure 6.12b - K^+K^- from the D_S^+ Signal Region

The relevant number of particles detected, and the efficiencies of detection are summarized in *Table 6.8*.

	D_S^-	D_S^+	Average
$D_S^\pm \to \phi\pi^\pm$ 'with sidebands'	321±24	313±24	317±17
$D_S^\pm \to \phi\pi^\pm$ '2xsidebands'	40±14	29±11	35±9
$D_S^\pm \to \phi\pi^\pm$	301±25	299±25	300±18
$D_S^\pm \to f_0(980)\pi^\pm$	39±63	79±64	59±45

Table 6.8 - Numbers of $D_S^\pm \to \phi\pi^\pm$ and $D_S^\pm \to f_0(980)\pi^\pm$ Found in Data

Chapter 7 - Conclusion

Recall *Equation (4.2)*:

$$\frac{BR\left(D_S^\pm \to f_0(980)\pi^\pm\right)}{BR\left(D_S^\pm \to \phi\pi^\pm\right)} \cdot \frac{BR\left(f_0(980) \to K^+K^-\right)}{BR\left(\phi \to K^+K^-\right)} = \frac{\#of\left(D_S^\pm \to \phi\pi^\pm\right)}{\#of\left(D_S^\pm \to f_0(980)\pi^\pm\right)} \cdot \frac{\varepsilon_\phi}{\varepsilon_{f_0(980)}}$$

Collecting numbers from *Tables 6.6, 6.7*, and *6.8* the final result is presented in *Table 7.1*.

	D_S^-	D_S^+	Average
$\dfrac{\#(D_S \to f_0(980)\pi)}{\#(D_S \to \phi\pi)}$	0.13±0.21	0.26±0.22	0.20±0.15
$\dfrac{\varepsilon_\phi}{\varepsilon_{f_0}}$	2.31±0.26	2.66±0.48	2.49±.27
$\dfrac{BR\left(D_S^\pm \to f_0(980)\pi^\pm\right)}{BR\left(D_S^\pm \to \phi\pi^\pm\right)} \cdot \dfrac{BR\left(f_0(980) \to K^+K^-\right)}{BR\left(\phi \to K^+K^-\right)}$	0.30±0.48	0.70±0.60	0.50±0.38

Table 7.1 - $\dfrac{BR\left(D_S^\pm \to f_0(980)\pi^\pm\right)}{BR\left(D_S^\pm \to \phi\pi^\pm\right)} \cdot \dfrac{BR\left(f_0(980) \to K^+K^-\right)}{BR\left(\phi \to K^+K^-\right)}$ and Intermediate Quantities

In conclusion, the product of the ratio of branching ratios is clearly consistent with zero, as the K^+K^- invariant mass plots indicate due to the lack of an obvious $f_0(980)$ signal. But recall *Figures 4.1* and *4.2*. Unlike the standard, well-above threshold decay which generates an obvious Breit-Wigner peak, *e.g.* $\phi \to K^+K^-$, the below threshold $f_0(980) \to K^+K^-$ rises very quickly to some maximum value, and then slowly drops. And in the invariant mass range of interest here (.95< K^+K^- <1.15)GeV, *Figures 4.2* shows that the $f_0(980)$, if present at all, rises to its maximum in the first few bins above its threshold, and

then drops to less than half of this maximum by the 1.15 GeV endpoint of this range. So, in K^+K^- invariant mass plots presented here, there would be one or two $f_0(980)$ in each of the first bins above threshold, and then there would be one or zero $f_0(980)$ in every bin thereafter. This is why the $f_0(980) \to K^+K^-$ decay mode is such a hard one to study.

As a final note, the errors reported in *Table 7.1* are strictly statistical. And because they are on the same order of the central value, not much effort has been given to quantifying sources of systematic error. However, the largest sources of systematic error are likely: first, the WA76 lineshape of the $f_0(980) \to K^+K^-$, and second, the efficiency calculation based on Monte Carlo simulation of the $f_0(980) \to K^+K^-$ decay using the WA76 lineshape.

Chapter 8 - Suggestions for Further Studies

This Master's Thesis obviously falls short of the full study of the $f_0(980)$ which could be done using the E791 data set - a list of studies to be added in a doctoral dissertation would include at least the following:

1. The data strip used here was one optimized by N Witchey [Witchey] to look for FCNC in $D_S^\pm$ - this yields good numbers of $D_S^\pm \to f_0(980)\pi^\pm$, but work needs to be done to optimize the $f_0(980)$ signal itself.

2. The present study looks only at the $f_0(980) \to K^+K^-$ decay mode, and only from resonant $D_S^\pm \to \left(f_0(980) \to K^+K^-\right)\pi^\pm$; in a hadroproduction experiment, there should be $f_0(980)$ produced from many other heavier/charm primary particles and $f_0(980)$ produced itself as a primary particle from beam/secondary target interaction. Furthermore, the $f_0(980)$ has $\pi^+\pi^-$, $\gamma\gamma$ and e^+e^- decay modes (though the latter two are greatly suppressed). All these sources of $f_0(980)$ and all its decay modes should be included in a comprehensive study of the particle.

3. A algorithm for 'automation' of the Dalitz-plot interference studies has been developed by R Greene and should be investigated as means to identify more precisely the $f_0(980)$ in any future study; see [Greene].

4. In both this study and R Greene's PhD Thesis, the parameterization of the $f_0(980)$ developed by the CERN WA76 experiment/collaboration was used to fit the K^+K^- spectrum and to generate the $f_0(980) \to K^+K^-$ Monte Carlo. A full $f_0(980)$ study, undertaking the above suggestions would be in a position to develop a new or better parameterization of the $f_0(980)$.

References

Barnes, T. *Proceedings of the Fourth Workshop on Polarized Targets Materials and Techniques*, Bad Honeff, Germany 1984, edited by W. Meyer (Bonn University, Bonn, 1984)

Gell-Mann, M. and Ne'eman, Y. *The Eightfold Way* (Benjamin, New York, 1964)

Greene, R. L. "Nonleptonic Decays of Charm Mesons", (University of Illinois at Urbana-Champaign, 1991).

Gribov, V. N. Lund Report No LU-TP-91-7 (1991).

Griffiths, D. Introduction to Elementary Particles (John Wiley & Sons, Inc, New York, 1987) 172.

Jaffe, R. L. Phys. Rev. Letters 41 (1975) 271.

Jaffe, R. L. Phys. Rev. D 15 (1977) 267.

Morgan, D. and Pennington, M. R. Phys. Rev. D48 (1993) 1185.

Morgan, D. and Pennington, M. R. Phys. Letters. 51B (1974) 71.

Robson, D. Nucl. Phys. B130 (1977) 328.

Sjostrand, T. *Pythia 5.7 and Jetset 7.4, Physics and Manual* (CERN, Geneva, 1993)`

Törnqvist, N. Phys. Rev. Letters 49 (1982) 624.

WA76 Collaboration. Armstrong, T. A., *et. al.* Z. Phys. C51 (1991) 351.

Weinstein, J. and Isgur, N. Phys. Rev. Letters 48 (1982) 659.

Witchey, N. J. "Search for Flavor Changing Neutral Current Decays of Charm Mesons" (Ohio State University, 1996)